Chapter 1

Introduction and literature review

Magnetic shape memory alloys (MSMAs) have garnered significant attention due to their substantial, rapid, and reversible magnetic field-induced strain (MFIS), making them highly suitable for applications in magnetic sensors and actuators [1–4]. As a result, MSMAs have emerged as a promising alternative to conventional shape memory alloys (SMAs), offering superior MFIS and faster response times, which are particularly advantageous for actuator applications [1]. Beyond their large MFIS, MSMAs exhibit a variety of extraordinary phenomena, including a pronounced magnetocaloric effect [5], giant magnetoresistance [6], anomalous thermal properties [7], exchange bias effect [8], spin-glass behavior [9], strain glass behavior [10], skyrmions [11], giant Hall effect [12], and anomalous Nernst effect [13], all of which hold considerable promise for technological applications. The present thesis investigates the structural, magnetic, magnetocaloric, and transport properties of prominent MSMAs, including $Ni_2Mn_{1.4}In_{0.6}$, $Ni_{1.9}Pt_{0.1}Mn_{1.4}In_{0.6}$, and $Ni_{50}Mn_{34}In_{16-x}Al_x$ (x =0.8), as well as the related hexagonal PtMnGa system.

1.1 Shape memory alloy

A SMA is a type of material that has the ability to "remember" its original shape and return to it when exposed to specific stimuli, such as thermomechanical or magnetic changes. This phenomenon is referred to as the shape memory effect (SME). In 1932, Arne Ölander discovered SMAs and observed their unique ability to return to a pre-defined shape when subjected to heating [14]. Later, in 1941, scientist Vernon was the first to use the term "shape memory" to describe his polymeric material [15]. Over time, the concept of shape memory was extended to metallic alloys, leading to the development of modern SMAs. The practical significance of SMAs became clear in 1962 when W. Buehler and F. Wang demonstrated the SME in a nickel-titanium (NiTi) alloy [16, 17], which later became widely known as Nitinol, a name derived from "NiTi" and the Naval Ordnance Laboratory. Since this discovery, the use of SMAs has expanded rapidly, finding widespread applications across various fields, including structural materials and composites [18], the automotive industry [19, 20], aerospace [21–24], mini actuators and microelectromechanical systems [25, 26], robotics [27, 28], and biomedical applications [29, 30]. Among

these, NiTi-based SMAs are the most extensively researched and widely used, owing to their outstanding performance and reliability [31].

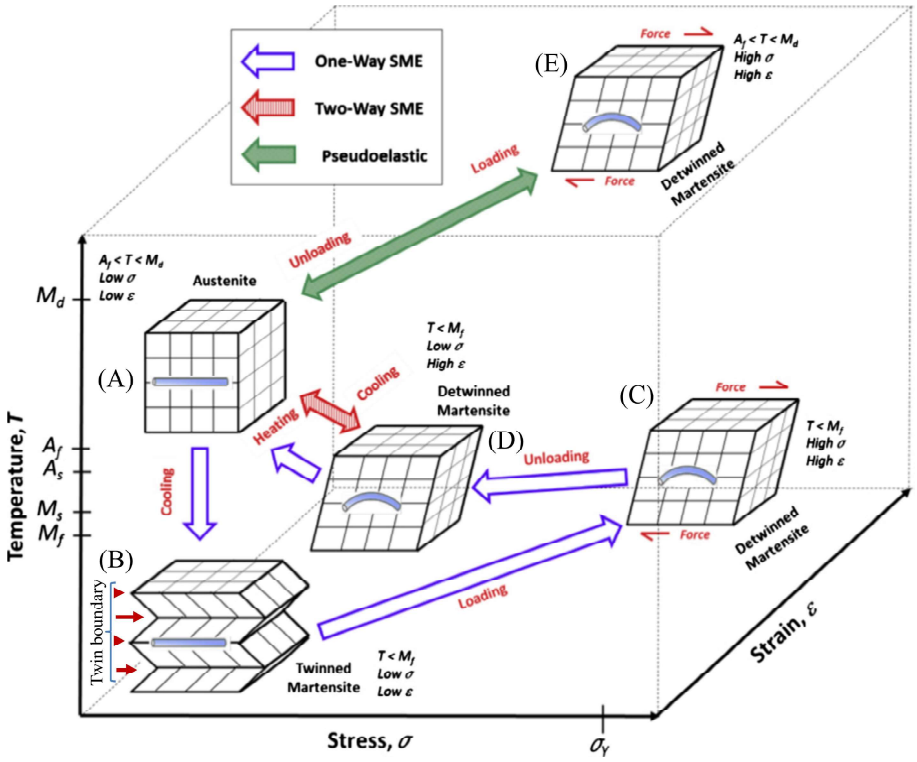

Figure 1.1: Phase transformations in shape memory alloy (SMA) [32].

In practice, SME is driven by a reversible phase transformation known as the martensite transformation (for further details, see Section 1.2). During this transformation, SMAs can exist in two distinct phases (named as, austenite and martensite), with three different crystal phases: twinned martensite, detwinned martensite, and austenite [33, 34] (Fig. 1.1). The austenite phase is stable at higher temperatures, while the martensite phase is stable at lower temperatures. As the SMA cools, the transformation starts from austenite to martensite at the martensite start temperature (M_s) and completes when the martensite finish temperature (M_f) is reached [16]. Upon heating, the material begins to revert from martensite to the austenite phase. The austenite-start temperature (A_s) marks the beginning of this transformation, while the austenite-finish temperature (A_f) indicates when the transformation is complete. When an SMA is heated beyond the A_s, it starts to distort and transform back into the austenite phase, recovering its original shape. This process can occur even under significant applied loads, resulting in high actuation energy densities [35].

The maximum temperature at which martensite can no longer be stress-induced is known as the martensite-deformation temperature (M_d). Above this temperature, the SMA behaves like a conventional metallic material and becomes permanently deformed [36]. The shape-changing effects are categorized into three distinct shape-memory characteristics, as detailed below:

(1) One-way shape memory effect: A one-way shape memory alloy (OWSMA) retains its deformed state after the external force is removed but recovers its original shape upon heating. This transformation is depicted in Fig. 1.1, illustrating the sequence from state A to D and back to A. When the austenite phase (state A) is cooled below M_s, it transforms into a twinned martensite phase. In the twinned martensite phase, variants with different crystallographic orientations coexist, as shown in state B. Twinning helps to accommodate strain energy in the martensite while maintaining an undistorted interface between the martensite variant and the parent phase. This undistorted interface is known as the invariant or habit plane. Applying an external load to one of the martensite variants in state B causes the variants to align along the load direction through twin boundary motion, producing a detwinned martensite state (state C) with significant shear strain. Upon removal of the load, state C does not revert to the twinned state. However, heating above A_f restores state C to its original austenite phase (state A).

(2) Two-way shape memory effect: In contrast to the one-way effect, a two-way shape memory alloy (TWSMA) can return to its original shape at both high and low temperatures. The transformation between states A and D is shown in Fig. 1.1. However, TWSMAs are less frequently used in commercial applications due to the need for extensive "training" and their generally lower recovery strain about half of that exhibited by OWSMAs of the same material [37, 38]. Moreover, their strain performance tends to deteriorate rapidly, particularly at higher temperatures [39].

(3) Pseudoelasticity (PE) or Superelasticity (SE): At temperatures between A_f and M_d, the SMA recovers its original shape upon the application of mechanical loading, without the need for thermal activation. This pseudoelastic behavior is shown between states A

and E in Fig. 1.1.

1.2 Martensite transformation

Martensite transformation (MT) is a solid-state phase transformation that occurs between two solid phases: the high-temperature phase, called austenite, and the low-temperature phase, known as martensite. In austenite, the crystal structure is typically cubic, whereas martensite has a more complex, lower-symmetry structure, such as monoclinic/tetragonal/orthorhombic. For example, in the Ni-Mn-based alloy, the cubic austenite phase transforms into a tetragonal martensite phase, characterized by the c/a ratio (referred to as tetragonality, where c and a are lattice parameters) [40]. This transformation is diffusion-

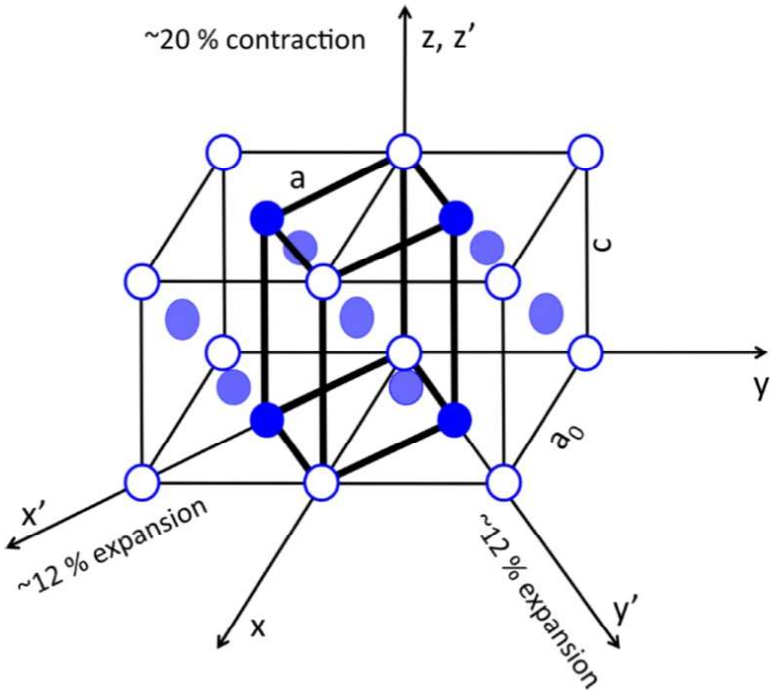

Figure 1.2: A schematic diagram of face-centered cubic (FCC) austenite to body-centered tetragonal (BCT) martensite transformation via Bain distortion [41].

less, as atomic diffusion is restricted as a result of both the low temperature and the rapid nature of the process, which can be close to the speed of sound in metals. Consequently, the parent and product phases retain identical chemical compositions. The Bain model is commonly used to describe martensite transformation in steels, where the face-centred cubic (FCC) to body-centered tetragonal (BCT) transformation occurs through a 20% con-

traction along the z-axis and a 12% expansion along the x- and y-axes [41] (as shown in Fig. 1.2). MT is classified as a first-order transformation, occurring through a nucleation and growth mechanism [42, 43]. Since MT involves a shape change, considerable strain develops around the martensite as it forms within the parent phase. Minimizing this strain is crucial for the nucleation and growth of the martensite. This is achieved either by introducing slip or by introducing twins, as shown in Figs. 1.3(b,c). These mechanisms are

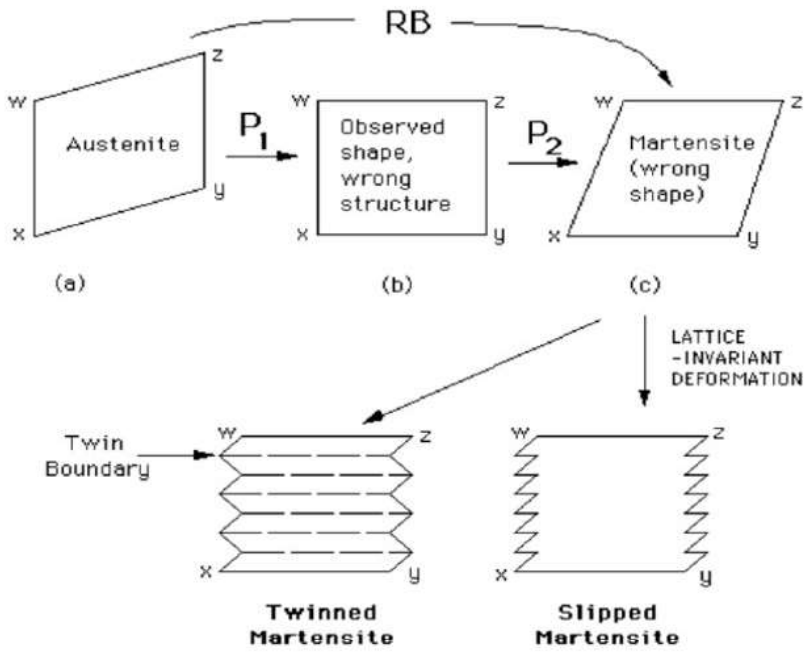

Figure 1.3: The diagram schematically illustrates the need for lattice invariant shear during martensite transformation: (a) shows the shape change during the transformation, while (b) and (c) depict how strain is accommodated by introducing slip (b) or twinning (c), respectively [41].

known as lattice invariant shear (LIS), as neither process alters the structure of the martensite. In other words, slip or twinning is a key element of MT. Twins or dislocations are frequently observed in martensites under electron microscopy, with the choice between slip or twinning depending on the specific alloy. Twinning is the dominant deformation mechanism in materials that possess low symmetry and large lattice parameters, as it effectively accommodates the strain induced during transformation. In twinned martensite, the interface between the martensite and austenite phases remains coherent, preserving the crystallographic alignment between them. This coherence is essential for the stability of the martensite phase and allows for efficient energy transfer during the transformation

process [44]. Moreover, the martensite transformation is generally athermal, characterized by rapid nucleation and growth, with the amount of transformed martensite being solely dependent on temperature [45]. However, in certain cases, the transformation can also be isothermal, depending on time [46, 47]. MT plays a crucial role in various applications, including steel hardening [48, 49], ceramic modification [47], and shape memory alloys [43]. The thermodynamic aspect of the martensite transformation is discussed, not-

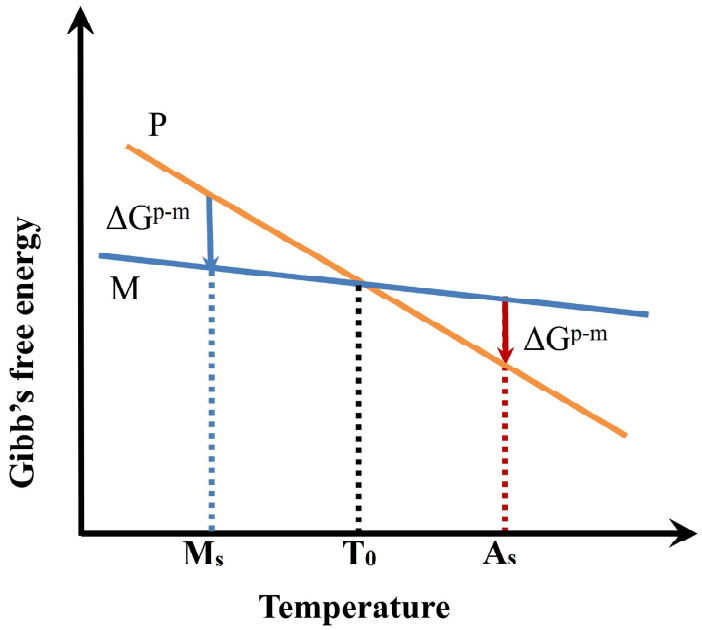

Figure 1.4: Schematic illustration of the free energy curves for both the parent (p) and martensite (m) phases [46].

ing that since MT does not involve a change in composition, the free energy curves of both the parent and martensite phases as a function of temperature are schematically depicted in Fig. 1.4. Here, T_0 represents the thermodynamic equilibrium temperature between the two phases. The term $\Delta G^{p-m} = G^m - G^p$ denotes the driving force for martensite nucleation, where G^m and G^p are the Gibbs free energies of the martensite and parent austenite phases, respectively [46]. When an SMA is cooled below a critical temperature, known as the martensite start temperature (M_s), the austenite phase transforms into martensite. This transformation is reversible; upon heating above the austenitic start temperature (A_s), the martensite reverts back to austenite. The specific temperatures, such as M_s and A_s, at which these transformations occur, are influenced by the alloy composition and processing

conditions.

1.3 Magnetic shape memory alloy

MSMAs represent an exciting class of smart materials that exhibit the ability to change shape in response to an applied magnetic field. This property, known as the magnetic shape memory effect (MSME), distinguishes MSMAs from conventional SMAs, which rely primarily on thermal or stress-induced phase transformations. MSMAs, also known as ferromagnetic shape memory alloys (FSMAs), are characterized by their ferromagnetic properties. They possess a magnetic moment that aligns with an external magnetic field. FSMAs can operate at higher frequencies, reaching up to 1 kHz, as their actuation energy is transmitted through magnetic fields, which are not affected by the slower heat transfer process [50]. The strain rate of FSMAs is comparable to that of magnetostrictive and piezoelectric active elements, while achieving strains as large as those of SMAs [39]. FSMAs can deliver the same specific power as SMAs but at higher frequencies [39]. The primary advantage of MSMAs is their ability to generate large strains (up to 10% in some cases) quickly and efficiently via magnetic activation, a process that is often faster and more controllable than thermal activation [3, 51–53]. FSMAs can achieve a maximum strain that is 32 times greater than the giant magnetostrictive material Terfenol-D ($TbDyFe_2$), with the trade-off being a 46 times lower elastic modulus (stiffness) [51]. As such, FSMAs are uniquely suitable to fill the technological gap between SMAs and magnetostrictive materials [55]. Figures 1.5(a-c) present a schematic representation of the MSME. In Fig. 1.5(a), a twinned martensite phase is depicted in the absence of a magnetic field. In this state, the twin variants are aligned according to their crystallographic orientation, and the magnetic spins are oriented along the easy axis of magnetization. When a magnetic field is applied (e.g., along the easy magnetization axis of a twin variant) to the twinned martensite phase, as shown in Fig. 1.5(b), the magnetic spins try to align with the direction of the applied field. Two conditions arise based on the interplay between magnetocrystalline anisotropy (MCA) and twinning stress (σ_t). Here, σ_t refers to the minimum stress or elastic energy required for twin boundary motion, while MCA, depicted in Fig. 1.5(d), is represented by

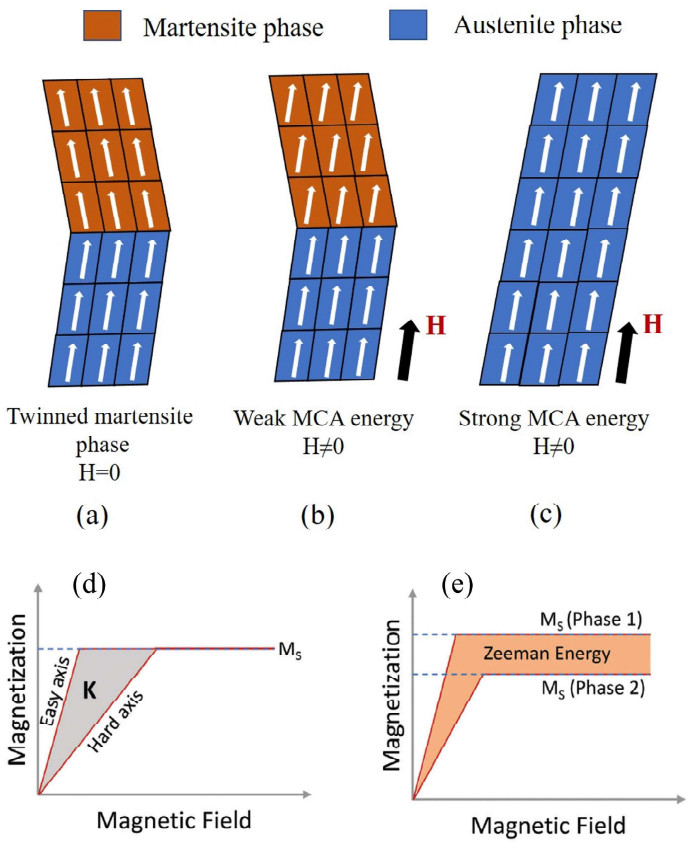

Figure 1.5: A schematic diagram illustrating the magnetic shape memory effect: (a) shows the martensite twin reorientation in the absence of a magnetic field (twinned martensite); (b) depicts the twin reorientation in the presence of a magnetic field with weak magnetocrystalline anisotropy; (c) shows the twin reorientation under a magnetic field with strong magnetocrystalline anisotropy (detwinned martensite); (d) represents the magnetocrystalline anisotropy; and (e) illustrates the difference in Zeeman energy between the austenite and martensite phases, which is responsible for the magnetic field-induced phase transformation (MFIPT) [54].

K.

Condition 1: If K, the MCA energy of the twin variants, is smaller than the energy required for twin boundary motion ($K < \sigma_t \epsilon_{max}$), where ϵ_{max} is the maximum attainable strain, the magnetic spins align with the field direction. However, the twin variant retains its original crystallographic orientation, resulting in no net change in the macroscopic shape, as illustrated in Fig. 1.5(b).

Condition 2: If $K > \sigma_t \epsilon_{max}$, the twin boundary moves along with the magnetic spin reorientation in the applied field direction. The twinned martensite transforms into a detwinned state. This transformation results in a large magnetic field-induced strain (MFIS)

and a corresponding net change in the macroscopic shape, as illustrated in Fig. 1.5(c).

The presence of sufficiently strong MCA ($K > \sigma_t \epsilon_{max}$) is the necessary condition for the MFIS. The difference between MCA energy and Zeeman energy of the adjacent martensite variants provides a driving force for twin boundary motion in the martensite phase. The Zeeman energy can be expressed by $E_{Zeeman} = \mu_0 H \Delta M$, where $\mu_0 H$ is magnetic field and ΔM is magnetization difference between the transformation phases (Fig. 1.5(e)). When the magnetic field is removed, the detwinned state does not spontaneously revert to the original twinned martensite state. To restore the twinned martensite state, an external stress (σ_{ext}) must be applied perpendicular to the direction of the magnetic field. This external stress acts as a restoring force to recover the original shape. Therefore, the condition for achieving reversible magnetic field-induced strain (MFIS) can be expressed as $K > (\sigma_t + \sigma_{ext})\epsilon_{max}$. It is important to note that the magnitude of σ_{ext} should not be so large as to impede the field-induced motion of the twin boundary. A critical value of external stress, referred to as the blocking stress, is required to ensure reversible MFIS.

1.4 Heusler alloys

Heusler alloys are a remarkable class of materials with distinctive properties and a wide range of applications. These alloys, named after the German mining engineer Friedrich Heusler who first discovered them in 1903, are especially notable for their ferromagnetism, despite being composed of non-magnetic elements [56]. Heusler alloys are classified into various types based on their crystal structures and constituent elements. The two most common categories are half-Heusler compounds (XYZ, with a 1:1:1 stoichiometric ratio) and full Heusler compounds (X_2YZ, with a 2:1:1 stoichiometric ratio) [57]. In these formulas, X and Y represent transition metals, while Z is a p-block (main group) element. The elements that can serve as the primary constituents of Heusler alloys from the periodic table are shown in Fig. 1.6 [57]. The half-Heusler compound adopts a cubic crystal structure, specifically belonging to the space group $F\bar{4}3m$. This structure is characterized by the arrangement of three interpenetrating FCC sublattices, as depicted in Fig. 1.7(a). In

this type of material, the X atoms are positioned at the $4c$ sites with coordinates $\left(\frac{1}{4}, \frac{1}{4}, \frac{1}{4}\right)$, while the Y atoms occupy the $4b$ sites with coordinates $\left(\frac{1}{2}, \frac{1}{2}, \frac{1}{2}\right)$, and the Z atoms are located at the $4a$ sites with the coordinates $(0, 0, 0)$. These positions are in accordance with the Wyckoff positions described for the respective atoms [57]. The unit cell of the half-Heusler compound, as shown in Fig. 1.7(b). The full Heusler compound crystallizes in the cubic space group $Fm\bar{3}m$. It consists of four interpenetrating FCC sublattices, as shown in Fig.1.7(c). As depicted in Fig. 1.7(d) the X atoms, typically transition metals, occupy tetrahedral sites within the crystal structure. These sites correspond to Wyckoff positions $8c$ with coordinates $\left(\frac{3}{4}, \frac{3}{4}, \frac{3}{4}\right)$. The Y atoms are located at the $4b$ position, with coordinates $\left(\frac{1}{2}, \frac{1}{2}, \frac{1}{2}\right)$, while the Z atoms occupy the $4a$ position, with the coordinates $(0, 0, 0)$.

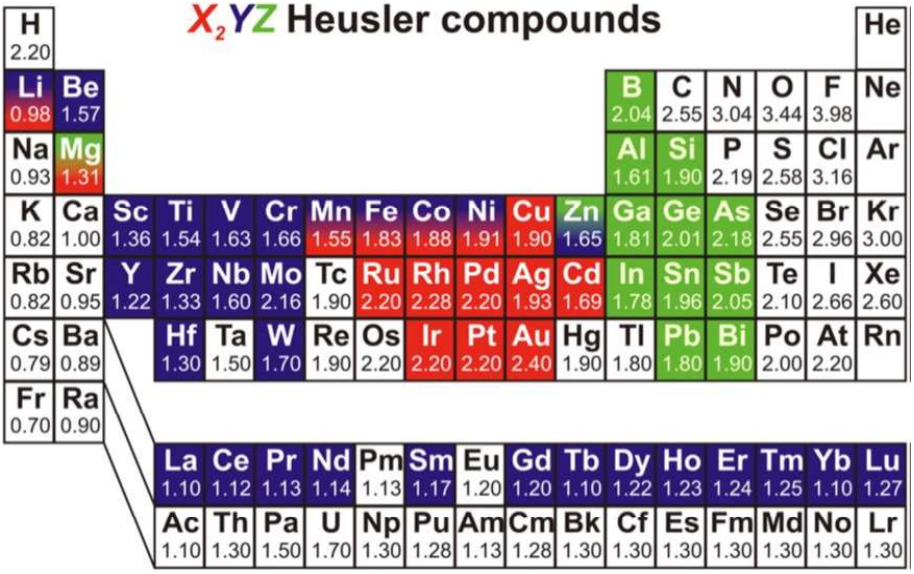

Figure 1.6: Periodic table of elements: A wide range of Heusler compounds can be formed by combining elements according to the color-coded scheme [57].

The magnetic properties of some Heusler compounds follow the Slater-Pauling rule, which is expressed as $m_{xyz} = N_v - 24$, where m represents the magnetic moment and N_v refers to the number of valence electrons [58]. As a result, a full Heusler compound with 24 valence electrons will display non-magnetic and superconducting characteristics. Similarly, the half-Heusler compound adheres to a variant of the Slater-Pauling rule, expressed as $m_{xyz} = N_v - 18$. For instance, TiCoSb, with 18 valence electrons, behaves as a diamagnetic semiconductor [57, 58]. By modifying the number of valence electrons, these materials can transform into ferromagnetic materials, such as VCoSb [57]. The flexibility

of Heusler compounds arises from their wide range of tunable band gaps, enabling them to exhibit properties such as topological insulators, metals, semimetals, half-metals, semiconductors, spin-gapless semiconductors, etc [59]. Ni-Mn-based Heusler compounds are a class of materials that exhibit remarkable scientific phenomena and fundamental properties, including superelasticity, giant caloric effects (magnetocaloric, barocaloric, and elastocaloric) [60, 61], spin glass behavior [9], large magnetoresistance [62], significant perpendicular magnetic anisotropy [63], large canting angles between magnetic moments [64], and exchange bias effects [65]. These properties make them highly promising for innovative applications in energy conversion, as well as in sensor and actuator devices [66]. These properties of Heusler compounds are linked to a first-order magnetostructural phase transition, where the high-temperature cubic austenite $L2_1$ phase transforms into a low-temperature martensite phase. The martensite phase at lower temperatures can vary in structure, depending on the composition, and may be tetragonal, orthorhombic, or monoclinic [57].

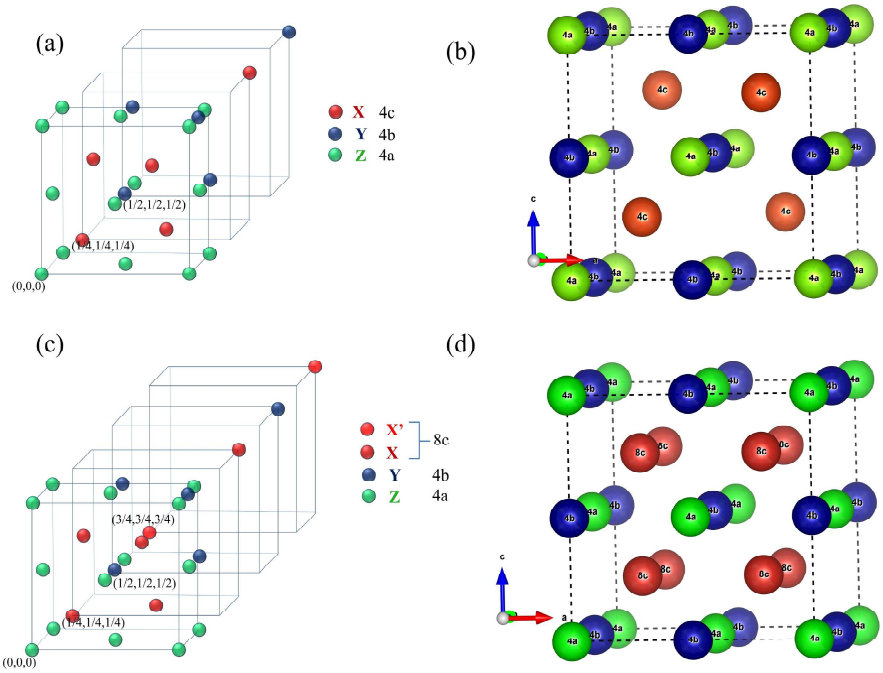

Figure 1.7: (a) Three interpenetrating face-centered cubic (FCC) sublattices. (b) The unit cell of half Heusler compound. (c) Four interpenetrating face-centered cubic (FCC) sublattices. (d) The unit cell of the full Heusler compound.

1.5 Magnetocaloric effect

The magnetocaloric effect (MCE) is the temperature change (heating or cooling) observed in a magnetic material when exposed to a changing magnetic field (ΔH) under adiabatic conditions. An illustration of MCE is shown in Fig. 1.8. MCE was first discovered by E.

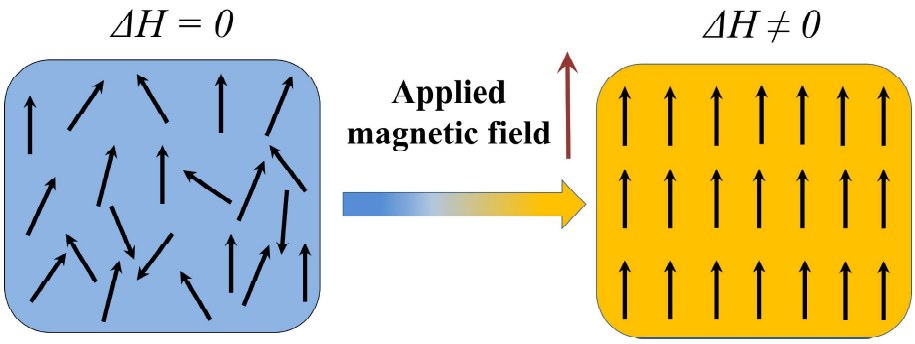

Figure 1.8: A schematic representation of magnetocaloric effect.

Warburg in 1881. Weiss and Piccard (1917) later observed the magnetocaloric effect at the ferromagnetic-to-paramagnetic second-order phase transition in elemental Ni [67, 68]. In 1926, Debye [69], and in 1927, Giauque [70], independently proposed the idea of achieving extremely low temperatures using adiabatic demagnetization as a cooling technique. This concept was successfully realized in 1933 when Giauque and MacDougall [71] conducted experiments that led to the development of the first functional adiabatic demagnetization refrigerator, capable of reaching temperatures as low as 0.25 K. Giauque was awarded the Nobel Prize in Physics in 1949 for his pioneering work on magnetic cooling. From 1933 to 1997, several advancements were made in utilizing the MCE for cooling applications [72, 73]. However, two major breakthroughs occurred in 1997. The first was a significant milestone achieved by Zimm et al. [74], who demonstrated that magnetic refrigeration is a practical and competitive cooling technology near room temperature, offering potential energy savings of up to 30%. The second breakthrough was the discovery of the giant MCE in $Gd_5(Si_2Ge_2)$ [75]. These two milestones sparked global interest among scientists and companies, leading to the development of new materials suitable for room-temperature applications and innovative magnetic refrigerator designs. The pursuit of higher-efficiency cooling and environmentally friendly magnetic refrigeration based on

the MCE has driven intensive research efforts. Beyond its practical applications, studies on the MCE also provide valuable insights into the nature of magnetic phase transitions [73, 76]. Most studies on the MCE have typically focused on calculating the isothermal entropy change (ΔS_{iso}) using indirect methods. However, for first-order phase transitions with thermal hysteresis, ΔS_{iso} can often be overestimated, requiring additional considerations [77]. Direct measurements of MCE provide adiabatic temperature change (ΔT_{ad}), a key parameter for magnetic refrigeration. Moreover, direct measurements more accurately reflect the actual processes used in practical applications. There are also other types of caloric effects based on the applied external fields, known as the "electrocaloric effect (ECE)" and the "mechanocaloric effect (mCE)". The ECE refers to the temperature change in materials under the application of an electric field in adiabatic conditions, while the mCE involves a temperature change in materials subjected to uniaxial stress or uniform pressure in adiabatic conditions. In practical applications, the efficiency of these materials (magnetocaloric, electrocaloric, and mechanocaloric materials) is characterized by the coefficient of performance (COP). The material-specific COP, denoted as COP$_{mat}$ (η), is defined as the ratio of latent heat (Q) to the input work (W) required to expel that heat. Carnot expressed η in terms of the hot (T_h) and cold temperatures (T_c) , as described in [78]:

$$\eta = \frac{T_c}{T_h - T_c} \tag{1.1}$$

Another important parameter is the specific heat of the materials (refrigerants). If a material has a high specific heat capacity, it requires more heat to increase its temperature and also releases more heat when cooling by the same temperature difference. To assess its effectiveness and suitability for cooling devices, researchers have introduced a dimensionless quantity, γ, defined as [78]:

$$\gamma = \frac{latent\,heat}{specific\,heat} \tag{1.2}$$

There are two cases depending on the value of γ. In the first case, if γ is high, heat can be easily extracted from the material using a heat exchanger. In the second case, if γ is

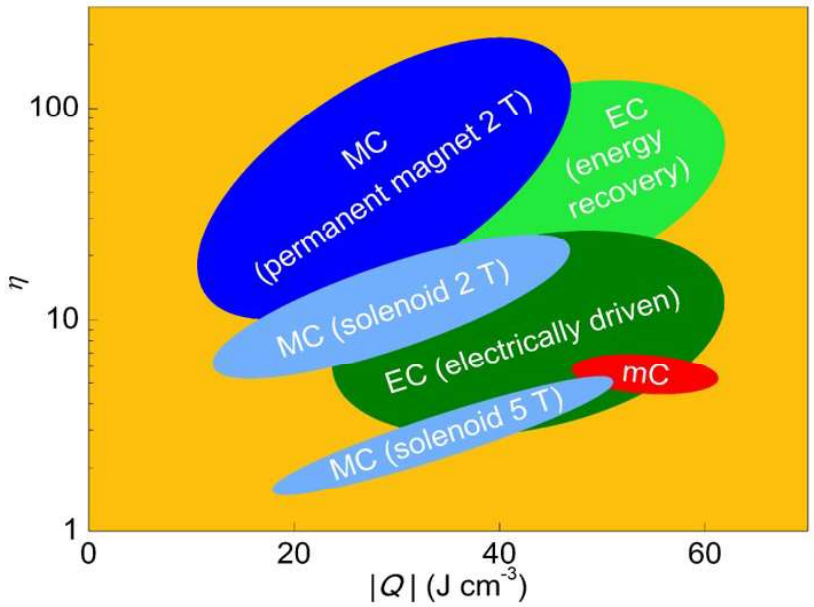

Figure 1.9: Comparison of the efficiency of various caloric materials (magnetocaloric, electrocaloric, and mechanocaloric) [5].

low ($\gamma \leq 1$), a more complex heat exchanger is required to extract heat from the material in cooling devices. For magnetocaloric materials, the efficiency (η) is higher compared to other caloric materials, as shown in Fig. 1.9. However, their γ value is lower than that of other materials, implying that a more complex heat exchanger is necessary to extract heat. Based on this analysis of the parameters, magnetocaloric materials are considered the best choice for cooling applications.

1.5.1 Thermodynamics of the magnetocaloric effect

The magnetocaloric effect originates in the ordering or randomization of the magnetic spin in magnetic materials. At constant pressure, the total entropy of solid magnetic material is the sum of magnetic (S_{mag}), lattice (S_{lat}) and electronic entropy (S_{elec}). Total entropy as a function of field and temperature can be written as:

$$S_{tot}(H,T) = S_{mag}(H,T) + S_{lal}(H,T) + S_{elec}(H,T) \tag{1.3}$$

Since magnetic entropy is due to the randomness of magnetic spin and after the application of the magnetic field, magnetic spin aligns in the direction of the magnetic field, and hence

magnetic entropy decreases. This decrease in magnetic entropy directly reflects on the total entropy if the field is applied in the isothermal condition since lattice entropy and electronic entropy are generally independent of the magnetic field. In adiabatic condition, total entropy should be constant ($\Delta S_{tot} = 0$), and therefore, change in magnetic entropy (ΔS_M or ΔS_{iso} after the application of the magnetic field would be compensated by the combined effect of lattice entropy and electronic entropy. Thus, with the decrease of the magnetic entropy, there would be an increase in lattice entropy in adiabatic condition and, hence, the temperature of the materials. This increase in temperature is called ΔT_{ad} of the materials. Fig. 1.10 illustrates the variation of entropy (S) with temperature (T) for MCE, highlighting a close relationship between ΔT_{ad} and ΔS_M in the graph. In this section,

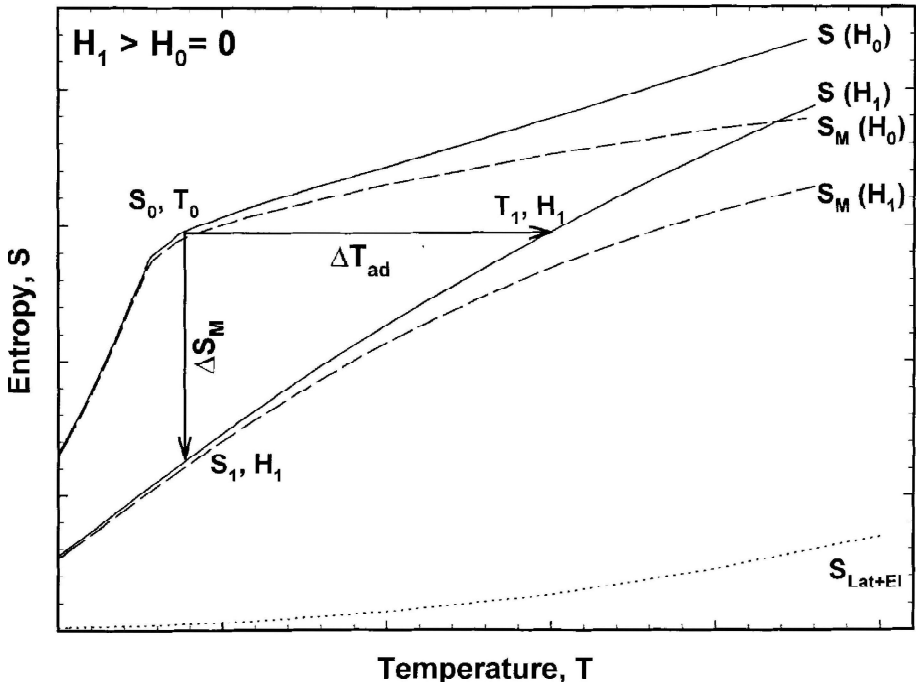

Figure 1.10: Illustration of magnetocaloric effect. It represents the total entropy change as a function of entropy change and adiabatic temperature change (ΔT_{ad}) when magnetic field changes from H_0 to H_1 [72].

we will derive a relation which connects the thermodynamic parameters to the magnetic parameter. A thermodynamic system is characterized by a set of thermodynamic variables such as pressure (p), temperature (T), internal energy (U), Gibbs free energy (G), column (V) etc. From the first law of thermodynamics, heat given to the magnetic system will increase the internal energy of the system, the system will work on the environment, and

magnetization of the system decreases due to the addition of the energy ($-\mu_0 HdM$) [79]. Hence,

$$dQ = dU + pdV - \mu_0 HdM \tag{1.4}$$

from the second law of thermodynamics,

$$dQ = TdS \tag{1.5}$$

comparing Eq. 1.4 and Eq. 1.5, we get-

$$TdS = dU + pdV - \mu_0 HdM \tag{1.6}$$

rearranging the Eq. 1.6, the change in U can be written as

$$dU = TdS - pdV + \mu_0 HdM \tag{1.7}$$

Internal energy in Eq. 1.7 contains the entropy term, and entropy is neither directly measured nor an easily controllable parameter. So it is required to express the energy in the form of measurable and easily controllable parameters. Gibbs free energy is expressed as-

$$G = U + pV - TS - \mu_0 HdM \tag{1.8}$$

differentiating Eq. 1.8 and replacing the dU from equation Eq. 1.7, the differential of Gibbs free energy is expressed as-

$$dG = dU + pdV + Vdp - (TdS + SdT) - (\mu_0 HdM + \mu_0 MdH) \tag{1.9}$$

$$dG = TdS - pdV + \mu_0 HdM + pdV + Vdp - TdS - SdT - \mu_0 HdM - \mu_0 MdH \tag{1.10}$$

$$dG = -SdT + Vdp - \mu_0 MdH \tag{1.11}$$

We can get different order parameters like S, V and M by taking the partial differential of Eq. 1.11 with respect to T, p and H, respectively. Hence we get,

$$S = -\left(\frac{\partial G}{\partial T}\right)_{P,H} \tag{1.12}$$

$$V = \left(\frac{\partial G}{\partial P}\right)_{T,H} \tag{1.13}$$

$$M = -\left(\frac{\partial G}{\mu_0 \partial H}\right)_{P,T} \tag{1.14}$$

From the partial differential theorem of calculus, it is known that second-order partial derivative results in the same value independent of the sequence of the variables. Differentiate partially S and M with respect to H, T respectively and using the above theorem, we get,

$$\left(\frac{\partial S}{\partial H}\right)_T = \mu_0 \left(\frac{\partial M}{\partial T}\right)_H \tag{1.15}$$

Eq. 1.15 is called Maxwell's relation, and after integrating this equation within the limit initial field (H_i) to the final field (H_f), we get,

$$\Delta S_{iso}(T, H) = \mu_0 \int_{H_i}^{H_f} \left(\frac{\partial M}{\partial T}\right)_{P,H} dH \tag{1.16}$$

From Eq. 1.16, we can see that the isothermal entropy change directly depends on the field change and the rate of magnetization change with temperature. Since total entropy is a function of field and temperature. Therefore, the differential form of S_{total} is as follows:

$$dS = \left(\frac{\partial S}{\partial T}\right)_{P,H} dT + \left(\frac{\partial S}{\partial H}\right)_{T,H} dH \tag{1.17}$$

for adiabatic process; $dS = 0$, from Eq. 1.17

$$0 = \left(\frac{\partial S}{\partial T}\right)_{P,H} dT + \left(\frac{\partial S}{\partial H}\right)_{T,H} dH \tag{1.18}$$

Heat capacity (C) is defined as the heat required to increase the temperature of the material by 1 K. Mathematically, it can be written as-

$$C = \frac{\partial Q}{\partial T} \tag{1.19}$$

using Eq. 1.5 in Eq. 1.19, we get

$$C = T\frac{\partial S}{\partial T} \tag{1.20}$$

Eq. 1.18 can be simplified by using Eq. 1.15 and Eq. 1.20

$$dT = -\mu_0 \frac{T}{C_{P,H}} \left(\frac{\partial M}{\partial T}\right)_{P,H} dH \tag{1.21}$$

Now, temperature change after applying the magnetic field in adiabatic condition can be determined by integrating the Eq. 1.21 from H_i to H_f. Hence,

$$\Delta T_{ad} = -\mu_0 \int_{H_i}^{H_f} \frac{T}{C_{P,H}} \left(\frac{\partial M}{\partial T}\right)_{P,H} dH \tag{1.22}$$

These two are important parameters (ΔS_{iso} and ΔT_{ad}) which determines the MCE. From both Eq. 1.16 and Eq. 1.22, it is clear that the value of MCE will be large if a change of magnetic field and the rate of change of magnetization with temperature are large. For the fixed value of the change in the field, $\left(\frac{\partial M}{\partial T}\right)$, $|\Delta T_{ad}(T,H)|$ will be larger as temperature increases. Materials having a lower value of heat capacity will result in a larger value of $|\Delta T_{ad}(T,H)|$.

1.5.2 Magnetocaloric effect at phase transitions

Based on the magnetic phase transition of materials and the sign (positive or negative) of ΔT_{ad} and ΔS_{iso}, the MCE can be classified into two types: “conventional” and “inverse” MCE.

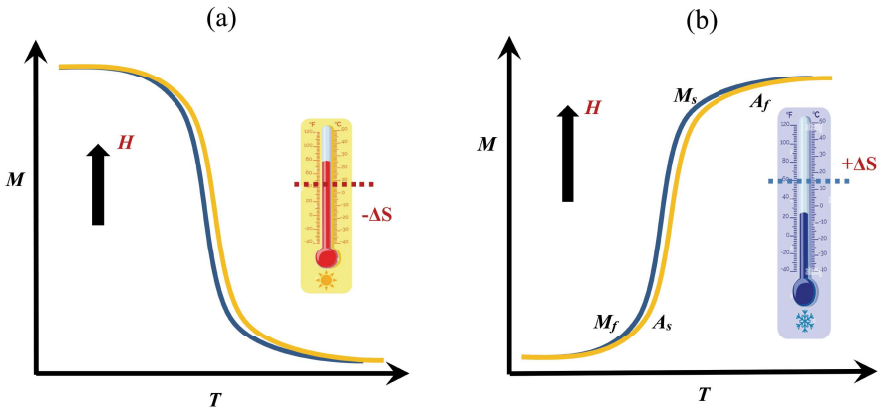

Figure 1.11: (a) Magnetization as a function of temperature $[M(T)]$ at a constant field (H) (a) demonstrating conventional caloric effect. (b) demonstrating inverse caloric effect.

1.5.2.1 Conventional magnetocaloric effect

In this effect, the material exhibits a decrease in magnetic entropy and a corresponding increase in temperature when subjected to a driving magnetic field under adiabatic conditions (i.e., $\Delta T_{ad} > 0$, $\Delta S_{iso} < 0$). This phenomenon occurs in materials where magnetization increases as the temperature decreases, particularly during a phase transition such as the paramagnetic-to-ferromagnetic transition. Examples of materials exhibiting this effect near their Curie temperature include Gd [80], $Gd_5Si_2Ge_2$ [75], $MnAs_{1-x}Sb_x$ [81], and $Ni_{55}Mn_{20}Ga_{25}$ [82], etc. A schematic representation of the magnetization vs. temperature curve is shown in Fig. 1.11(a).

1.5.2.2 Inverse magnetocaloric effect

In this effect, the material exhibits an increase in magnetic entropy and a corresponding decrease in temperature when subjected to a driving magnetic field under adiabatic conditions (i.e., $\Delta T_{ad} < 0$, $\Delta S_{iso} > 0$). This phenomenon occurs in materials where magnetization decreases as the temperature decreases at their magnetostructural phase transition. Examples of materials exhibiting this effect near their martensite phase transition include $Ni_{50}Mn_{37}Sn_{13}$ [83], $Ni_{45.2}Mn_{36.7}In_{13}Co_{5.1}$ [60], $Fe_{49}Rh_{51}$ [84], etc. A schematic representation of the magnetization vs. temperature curve is shown in Fig. 1.11(b).

1.5.3 Measurement of magnetocaloric effect

1.5.3.1 Direct measurements

The direct measurement of MCE involves determining the temperature change of a material when exposed to a finite magnetic field under adiabatic conditions. For such measurements, the temperature change of the sample can be monitored using two primary techniques:

1. Contact techniques: These require direct thermal contact between the sample and the temperature sensor, such as thermocouples or thermistors. They are well-suited for applications involving strong magnetic fields and significant temperature changes [85–87].

2. Non-contact techniques: Based on the thermoacoustic principle, these methods detect exponentially decaying pressure waves, generated by a sample with a periodically varying surface temperature, using a sensitive microphone. They are ideal for scenarios involving weak magnetic fields and small temperature variations [75, 88]. Direct measurements require adiabatic conditions, which necessitate a sufficiently rapid change in the magnetic field. Two commonly used methods for such measurements are:

a. Changing the magnetic field while keeping the sample fixed, such as by charging or discharging the magnet [86].

b. Moving the sample in and out of a constant magnetic field [87].

Electromagnets can generate magnetic field strengths of up to 2 T, while permanent and superconducting magnets typically operate within a range of 0.1–10 T [75]. In this thesis, the ΔT_{ad} of a Gd sample was measured directly using a contact technique. The sample's surface was connected to a PT100 sensor in homemade setups. In these systems, electromagnets produced magnetic fields up to 1 T, while a permanent magnet generated fields up to 0.5 T.

1.5.3.2 Indirect measurements

In indirect measurements, the MCE parameter (ΔT_{ad}) is indirectly determined through thermodynamic analysis of magnetization data and heat capacity measurements, specifically by calculating ΔS_{iso}. The indirect measurement of the MCE can be classified into two types of methods.

1. **Maxwell method:** In this method, the value of ΔS_{iso} is obtained by integrating the Maxwell equation within appropriate variable limits The Maxwell equation is expressed as [89]:

$$\left(\frac{\partial S}{\partial H}\right)_T = \left(\frac{\partial M}{\partial T}\right)_H \tag{1.23}$$

   where S represents entropy, T is temperature, H denotes the magnetic field, and M is magnetization. This approach is particularly effective for second-order transitions or first-order transitions with minimal hysteresis.

2. **Clausius-Clapeyron method:** This method is applicable exclusively to first-order transitions, particularly for samples with strong hysteresis [89]. The value of the MCE parameter can be determined using the Clausius-Clapeyron relation, expressed as:

$$\Delta S_{iso} = -\Delta M \left(\frac{dH}{dT}\right) \tag{1.24}$$

   where ΔM is the change in magnetization, and $\frac{dH}{dT}$ represents the slope of the magnetic field vs temperature curve.

1.5.3.3 Quasidirect methods:

In this method, the ΔS_{iso} is determined using heat capacity [90] and heat flux measurements [91]. This approach is particularly sensitive to first-order transitions. The two measurement methods are described below:

1. **Heat-capacity method:** The value of ΔS_{iso} is calculated by measuring the temperature-

dependent heat capacity under varying magnetic fields, expressed as:

$$\Delta S_{iso}(T, H_2 - H_1) = \int_{T_1}^{T_2} [C(T, H_2) - C(T, H_1)] \frac{dT}{T} \tag{1.25}$$

2. **Heat-flux method:** The value of ΔS_{iso} is determined by measuring the temperature-dependent heat flux as a function of the changing magnetic field, expressed as:

$$\Delta S_{iso}(T, H_2 - H_1) = \int_{T_1}^{T_2} \left[\frac{dQ}{dT}(T, H_2) - \frac{dQ}{dT}(T, H_1) \right] \frac{dT}{T} \tag{1.26}$$

Here, H_1 and H_2 represent the initial and final magnetic fields, T_1 is the temperature far from the transition region, T_2 is the final temperature, and $\frac{dQ}{dT}$ denotes the heat flux. The value of ΔT_{ad} cab be calculated using Eq. 1.22.

1.5.4 Magnetic refrigeration process

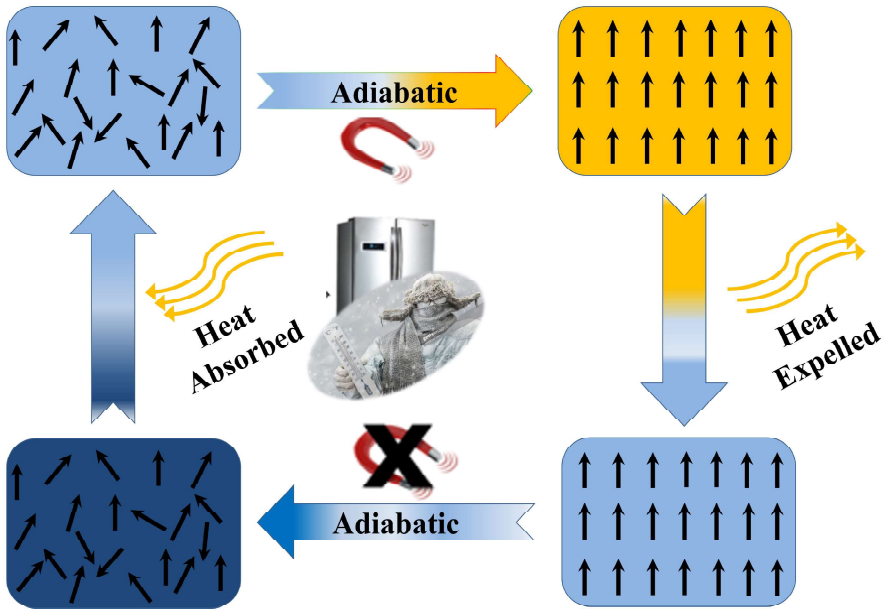

Figure 1.12: A schematic illustration of the four stages of the magnetic refrigeration cycle.

Magnetic refrigeration is an eco-friendly, efficient, and energy-saving cooling technology. It uses magnetic materials as refrigerants and a magnet to create a magnetic field. A heat transfer fluid, such as water or ethanol, transfers heat between the magnetic material and the system being cooled. The first magnetic refrigerator was developed at Ames Labo-

ratory, University of Iowa [92]. This prototype used gadolinium (Gd) as the magnetic material, a magnetic field strength of 1.5 T, and water as the heat transfer fluid. Gd-based magnetic refrigerants can achieve about 60% efficiency of the theoretical limit, which is higher than conventional gas refrigerators [72–74, 76]. The schematic diagram of magnetic refrigeration cycle is shown in Fig. 1.12. Magnetic refrigeration works through a four-step thermodynamic cycle based on the conventional caloric effect. In the first step (adiabatic magnetization), a magnetic field is applied to the magnetic material under adiabatic conditions, causing its temperature to increase. This occurs as the magnetic moments reorient and align with the direction of the applied field, reducing the magnetic entropy of the system. Since the total entropy remains constant, the lattice entropy and electronic entropy increase due to enhanced lattice vibrations, resulting in a temperature rise in the magnetic material. In the second step (isomagnetic cooling), the heat generated during the first step is released to the surroundings while the magnetic field remains constant. In the third step (adiabatic demagnetization), the material is demagnetized under adiabatic conditions, causing its temperature to decrease. Finally, in the fourth step (isomagnetic cooling), the cooled material absorbs heat from the system, lowering the temperature of system. This cycle is then repeated to maintain continuous cooling. Magnetic refrigeration eliminates the need for harmful refrigerant gases, reducing environmental impact. It offers greater energy efficiency compared to gas compression refrigeration. The technology is suitable for various applications, including domestic refrigeration and cryogenics. Materials with a strong magnetocaloric effect, such as Gd, are essential for efficient performance. Research continues to explore alternative magnetic materials for better cost-effectiveness. Enhancements in magnet design can further improve efficiency. The magnetic refrigeration cycle is promising for sustainable cooling solutions.

1.6 Transport properties

1.6.1 Anomalous Hall effect

In 1879, Edwin H. Hall observed that when a current-carrying conductor is placed in a perpendicular magnetic field, the magnetic field applies a Lorentz force on the moving charge carriers, causing them to deflect towards the transverse side of the conductor [93]. This generates a measurable transverse voltage known as the Hall voltage, and this phenomenon is called the Hall effect (HE). HE is a fundamental phenomenon in the field of condensed matter physics and serves as a vital experimental tool for determining the type of charge carriers, measuring carrier density, and assessing magnetic field strength [94]. A schematic diagram of the HE is shown in Fig. 1.13(a), while the variation of Hall resistivity (ρ_H) as a function of the magnetic field for the non-magnetic (NM) material is presented in Fig. 1.13(b). ρ_H under a magnetic field applied along the z-axis is given by $\rho_H = R_0 H$, where R_0 is the Hall coefficient. Under the free electron gas approximation, R_0 is related to the carrier density (n) by the expression $R_0 = -\frac{1}{ne}$ [94]. In 1880, Ed-

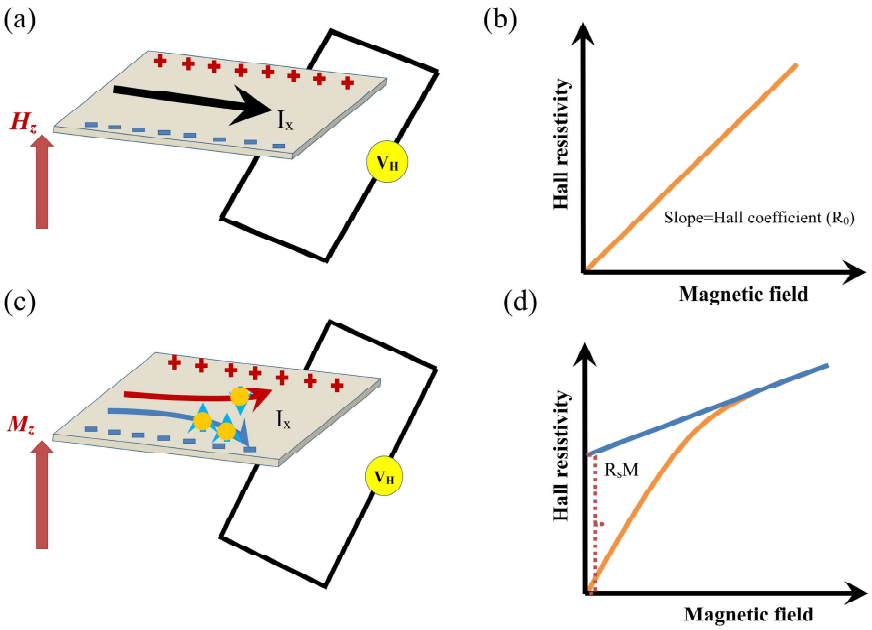

Figure 1.13: (a) Schematic diagram of Hall effect. (b) A typical Hall resistivity (ρ_H) as a function of magnetic field for a nonmagnetic conductor. (c) Schematic illustration of anomalous Hall effect (AHE). (d) A typical Hall resistivity (ρ_H) curve as a function of magnetic field for a ferromagnetic conductor, where $R_S M$ is the zero-field intercept [95].

win H. Hall further discovered a stronger presession of electrons in ferromagnetic (FM) conductors than in NM materials. This enhanced HE is named as anomalous Hall effect (AHE) [96]. Further experiments on materials such as Fe, Co, and Ni suggested that AHE was related to the magnetization of the sample [97]. An empirical formula for the total Hall effect in FM conductors can be written as [98–100]

$$\rho_H = R_0 H + R_S M \tag{1.27}$$

here, $R_S M$ represents anomalous Hall resistivity (ρ_{AH}), R_S is the anomalous Hall coefficient and M is the magnetization of the FM material. A schematic representation of the AHE is depicted in Fig. 1.13(c). In contrast to the NM conductors, FM conductors show non-linear behaviour in Hall resistivity (Fig. 1.13(d)). For FM conductors, ρ_H rises sharply at low magnetic fields due to the rapid saturation of magnetization. Once the magnetization saturates, ρ_H becomes linear (constant) with respect to H at higher fields, where the normal Hall contribution dominates. If this linear section is extrapolated back to zero field ($H = 0$), it will not pass through the origin. Instead, the y-axis intercept provides the value of $R_s M$, as described in Eq. 1.27. Although HE and AHE appear similar, their origins are different. HE arises from the Lorentz force acting on moving electrons in an external magnetic field, whereas AHE occurs without an external magnetic field. Since no magnetic field is present, the AHE is not caused by the orbital motion of electrons [94]. The origin of AHE has remained a puzzling issue since its discovery. A significant breakthrough in understanding this phenomenon was made by Karplus and Luttinger [101], who demonstrated that electrons moving under an external electric field can develop an "anomalous velocity" perpendicular to the field. This transverse velocity contributes to the lateral motion of electrons, thereby playing a key role in the AHE. The "anomalous velocity" is a result of the electron-filled states in FM conductors influenced by spin–orbit coupling (SOC). SOC is a relativistic phenomenon which occurs when an electron perceives a magnetic field in its rest frame due to the electric field created by a localized electron or magnetic impurity. The correlation induced by SOC influences electron trajectories and plays a role in the AHE [102]. It has been suggested that this mechanism

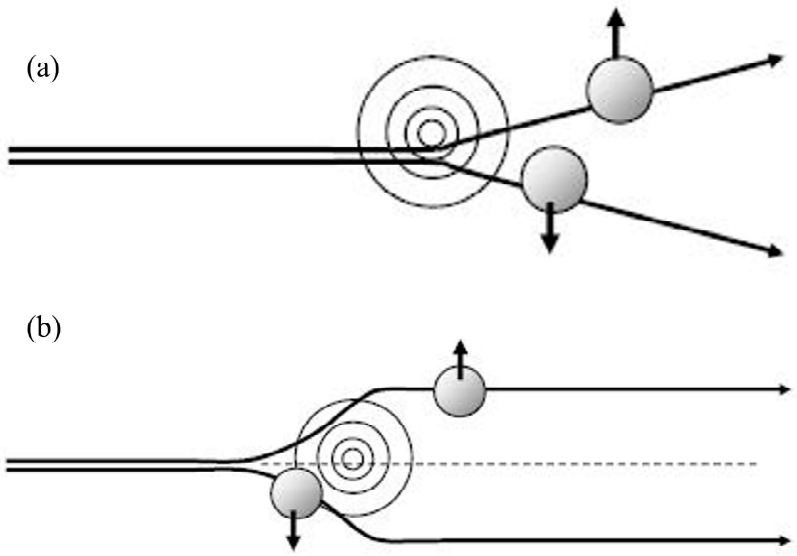

Figure 1.14: Schematic illustrations of (a) skew scattering and (b) side jump [94].

leads to ρ_{AH} proportional to the second power of the longitudinal resistivity ($\rho_{AH} \propto \rho_{xx}^2$). Since this contribution depends solely on the band structure of an ideal crystalline structure and is completely unaffected by scattering from impurities, it is responsible for the intrinsic AHE in materials [94, 103–105]. After some time, two extrinsic mechanisms (skew scattering and side jump) were identified as dominant contributors to the AHE. It was proposed that defects or impurities are inevitably present in actual materials and can deflect moving electrons [106, 107]. When both SOC and ferromagnetism are present in the material, the scattering of electrons becomes asymmetric, resulting in an unequal lateral motion of electrons. This phenomenon is referred to as skew scattering. [106]. A schematic diagram of this process is depicted in Fig. 1.14(a). Unlike the intrinsic contribution, this mechanism predicts $\rho_{AH} \sim \rho_{xx}$. Later, Berger [107] proposed that electrons encounter different electric field as they approach and depart from an impurity, leading to an extra asymmetric scattering mechanism known as side jump, which is an additional contributor to AHE. A schematic diagram of the side jump is depicted in Fig. 1.14(b). This mechanism surprisingly predicts $\rho_{AH} \sim \rho_{xx}^2$, which aligns with the intrinsic contribution. From an experimental perspective, defects or impurities in samples are inevitable and often exhibit varying levels of complexity. As a result, intrinsic and extrinsic mechanisms commonly act together in contributing to the AHE [108].

1.6.2 Topological Hall effect

Beyond the AHE, another intriguing topological Hall effect (THE) has garnered significant interest in recent years [109–112]. THE typically arises in magnetic materials with strong SOC and broken inversion symmetry, which are key factors in establishing the Dzyaloshinskii-Moriya interaction (DMI) [113, 114]. The competition of the DMI, symmetric exchange interactions such as Heisenberg exchange, and an applied magnetic field can support the formation of complex topological magnetic structures, which exhibit a finite Berry curvature [115, 116]. The origin and characteristics of the THE differ from those of the AHE, which is driven by uniform magnetization. THE arises from nonuniform, noncollinear magnetization, and specific chirality. It introduces an additional contribution to the total Hall signal, in combination with the normal Hall and anomalous Hall components [117]. This effect results from an induced magnetic field due to finite Berry phase contributions in real or momentum space when conduction electrons interact with a noncoplanar spin structure having finite chirality [118]. When the length scale of the magnetic texture is comparable to the to the periodicity of the crystal structure and much smaller than the electron's mean free path, the Berry curvature in momentum space becomes dominant. In this regime, the variation of the noncoplanar magnetic spin arrangement in weak external field replaces the role of SOC [119]. The induced emergent field arises from the cone angle formed by three spins, leading to scalar spin chirality, which can be expressed as $\chi_{ij} = \sum \vec{S}_i.(\vec{S}_j \times \vec{S}_k)$, where $\vec{S}_i$ represents the spin vector of a magnetic atom. The magnitude and direction of the emergent field in noncoplanar systems are influenced by the external magnetic field and show an approximately linear response to variations in the external field at a fixed temperature. In the case of real-space Berry curvature, where the magnetic texture length scale is much larger than the mean free path, THE arises from an adiabatic topological magnetic spin configuration. The topological nature of a spin configuration is characterized by a quantity called the topological winding number [112, 120], defined in terms of its scalar spin chirality. This number provides a measure of how spins are arranged in a noncoplanar configuration, capturing the degree of "twisting" or "winding" of the spin texture in space. In the continuum limit ($\vec{S}_i \rightarrow \vec{n}$), where $\vec{n}$ represents the

local unit vector of the magnetization direction, the topological winding number is expressed as an integral over the spin configuration. The emergent magnetic field generated by the real-space Berry curvature [121, 122] adiabatically deflects the spin-polarized motion of electrons, with opposite field directions acting on spins of opposite sign [122]. For skyrmionic textures, this emergent field remains constant. THE driven by real-space Berry curvature is independent of scattering and, as a result, remains constant with respect to longitudinal resistivity [123]. Taking the THE into account, the total Hall resistivity can be written as:

$$\rho_H = R_0 H + R_S M + \rho^T \tag{1.28}$$

here, ρ^T is the topological Hall resistivity. THE is an electrical transport property closely associated with skyrmions [112]. A magnetic skyrmion is a localized swirling spin configuration within a magnetic material [124]. The concept of skyrmions was first introduced by Tony Skyrme in the 1960s to explain the stability of hadrons in particle physics [125–127]. In this context, particles were described as quantized topological defects, whose stability is protected by a topological integer that remains unchanged under continuous deformations of the field configuration. Skyrmions were first experimentally observed in 2009 using neutron scattering in the chiral magnet MnSi [128]. There are three primary types of skyrmions, known as "Bloch-type", "Néel-type", and "antiskyrmion" distinguished by their different spin modulations along the radial direction (as illustrated in Fig. 1.15(a-c)). The schematic diagram of ρ^T as a function of the field is depicted in Fig. 1.15(d). The insets show the skyrmions at positive and negative fields. In Bloch-type skyrmions, the magnetic moments rotate perpendicular to the radial plane, while in Néel-type skyrmions, the moments rotate within the radial plane [129]. Furthermore, antiskyrmions exhibit a combination of both Bloch- and Néel-type magnetization dynamics [130]. In non-centrosymmetric materials, where symmetries can be schematically represented using molecular models, DMI plays a key role in the formation of skyrmions with fixed vorticity and helicity. Skyrmions in such systems have been observed in various materials, for example $Mn_{1-x}Fe_xGe$ [133], FeGe [134, 135], Cu_2OSeO_3 [136, 137], and $Co_8Zn_8Mn_4$ [138]. Later, skyrmions have also been detected in magnetic thin films de-

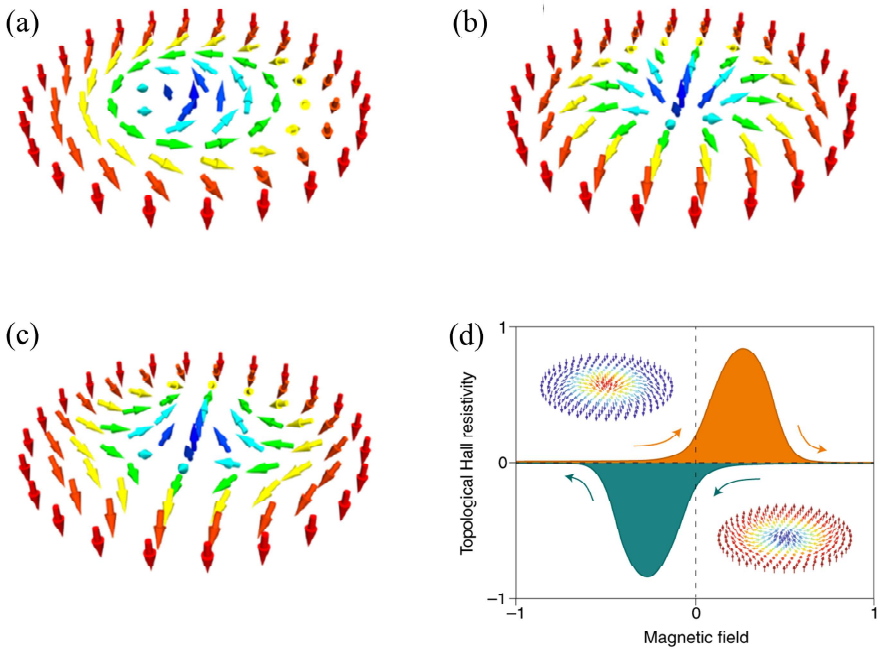

Figure 1.15: (a) Bloch Skyrmion. (b) Néel Skyrmion. (c) Antiskyrmion [131] (d) Topological Hall resistivity as a function of magnetic field. Insets show skyrmion textures within positive and negative magnetic fields [132].

posited on heavy metal substrates, where strong DMI emerges due to inversion symmetry breaking at the interface [139]. Skyrmions can also arise in centrosymmetric materials due to competing magnetic interactions, such as exchange interaction, magnetic anisotropy, and long-range dipolar interactions. Examples of centrosymmetric materials exhibiting skyrmionic structures driven by these competing forces include NiMnGa [140], Ni_2MnGa [11], $(Mn_{1-x}Ni_x)_{65}Ga_{35}$ [141], Fe_3Sn_2 [142, 143], Mn_4Ga_2Sn [144], $La_{1-x}Sr_xMnO_3$ [145], and Fe_3GeTe_2 [146] etc. The magnetic configurations of skyrmions give rise to nontrivial topological properties, often referred to as topological stability [147]. Notably, magnetic skyrmions can be controlled using various external stimuli, like electric currents in metals [148], electric fields in insulators [136], strain [149], and heat currents [150]. A key advantage of skyrmions is that the threshold current density required to move them is approximately three to five orders of magnitude lower than that needed to drive ferromagnetic domain walls [148]. These unique properties—including controllable ultra-small size, topological stability, and low-threshold current for motion—make skyrmions highly promising for the development of next-generation low-energy, high-density memory de-

vices where skyrmions serve as data bits [151–153].

1.7 Ni-Mn-In-based MSMAs (cubic austenite phase) and PtMnGa (hexagonal austenite phase)

In general, Ni-Mn-based Heusler alloys undergo a first-order magnetostructural phase transition at their martensite phase transition (T_M) [154, 155]. This phase transition gives rise to several important technological properties, including MCE [156], anomalous and topological Hall effects, Nernst effect [157], and large exchange bias [158], etc. The structure, magnetic transition temperatures, and related properties of these MSMAs are highly sensitive to the composition and the valence electron concentration per atom (e/a) ratio [159]. As shown in the phase diagram of Ni-Mn-In MSMAs in Fig. 1.16, M_s can be tuned within a range of approximately 200 K to 1000 K by adjusting the e/a ratio from about 7.85 to 8.5. The stoichiometric Ni_2MnIn MSMA does not exhibit martensite phase transition [160, 161], unlike other Ni-Mn-based Heusler alloys. Notably, when the Mn content is increased to a critical value (in the composition $Ni_2Mn_{1.36}In_{0.64}$), the martensite phase transition begins to appear [161]. Generally, the martensite phase in Ni-Mn-In MSMA displays a 3M, 5M, or 7M modulated monoclinic structure [162, 163]. The martensite phase of Ni-Mn-In MSMAs shows lower magnetization due to either paramagnetic (PM) or antiferromagnetic ordering [161], although the exact nature of this ordering remains unclear. Recent studies reported the observation of the premartensite phase (PM-phase) in Ni-Mn-In MSMAs [164]. The PM-phase has been identified as a crucial precursor to the martensite phase in these alloys [164]. In these materials, the transition to the martensite phase does not occur directly from the high-temperature cubic austenite phase. Instead, it is preceded by an intermediate PM-phase, which plays a significant role in the phase transformation process. Since the PM-phase is closely linked to the martensite phase and responsible for exhibiting the shape memory effect, it has garnered significant attention in these alloys. Researchers have focused on understanding the crystal structure, phase stabilities, structural modulation, and the relationship between structure and properties of

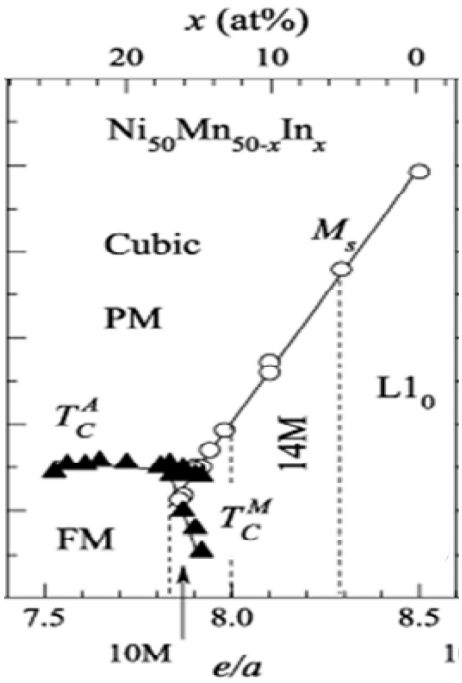

Figure 1.16: Phase diagram of $Ni_{50}Mn_{50-x}In_x$ magnetic shape memory alloy [159].

the PM-phase to better comprehend its role and influence in these materials [165–168]. Studies suggest that the PM-phase is directly associated with skyrmion formation (consequently, the transport properties) in Ni-Mn-In-based MSMAs [164], highlighting the importance of investigating the transport properties in these materials. However, only a few studies have focused on transport measurements, and the origin of these properties remains unclear [169–171]. Recent studies suggest that the PM-phase in Ni-Mn-In MSMAs can be stabilized through chemical pressure tuning [172, 173].

In addition to Ni-Mn-In-based MSMAs possessing a cubic austenite phase, there exists another category of materials with a hexagonal austenite phase [174] that also exhibit magnetic shape memory behavior [175]. These materials are half-Heusler compounds, known as Mn-based MnXY compounds, consist of X as a transition metal and Y as a group IIIA or IVA element [176]. Beyond their magnetic shape memory properties, these materials exhibit a range of intriguing physical phenomena, including MCE [177–179], magnetoresistance [180], and noncollinear magnetic structures [181]. Typically, these compounds undergo a structural transformation from a high-symmetry hexagonal (austenite) phase to a low-symmetry orthorhombic (martensite) phase [174, 182, 183]. Notably,

the martensite phase in these compounds exhibits a larger volume compared to the austenite phase [174]. The martensite phase in these materials can be suppressed by altering the composition through doping [174, 178], introducing an adequate concentration of vacancies [184], applying external pressure [185], or adjusting the e/a ratio [185]. Consequently, these materials can be categorized into two classes: those that exhibit a phase transition from hexagonal austenite to orthorhombic martensite and those with a stable hexagonal austenite phase only. Recently, compounds with a stable hexagonal austenite phase have garnered significant attention due to their fascinating non-coplaner spin configuration [186, 187]. In this thesis, the compound under investigation is PtMnGa, where Pt replaces X and Ga replaces Y in the XMnY half-Heusler compound [186]. PtMnGa exhibits bulk-type stable Néel skyrmions over a wide temperature range from 220 K to 5 K [186]. At room temperature, this compound exhibits PM behaviour. It transitions to a FM state at its $T_C \sim 236$ K. It exhibits a canted antiferromagnetic (CAFM) state at 175 K, resulting in a weak magnetization. This transition marks a significant change in the material's magnetic ordering. At 148 K, the system undergoes another transformation from the CAFM state to a complex phase that combines both the CAFM and spin density wave (SDW) states. The SDW state is characterized by the periodic modulation of the electron density [188]. These transitions underscore the complex interaction between the material's magnetic and structural properties, which are strongly affected by factors such as temperature and magnetostructural coupling [188]. Notably, in the PtMnGa system, it has been observed that T_C increases when subjected to hydrostatic pressure. This temperature shift occurs at a rate of $dT_C/dP = 1.7$ K/kbar [189], indicating that the application of pressure has a substantial impact on the material's magnetic properties. This suggests that there is a possibility to get the thermodynamically stable skyrmions temperature regime (210-220 K) close to room temperature or even at a higher temperature, which necessitates a detailed pressure-dependent structural investigation of the PtMnGa system. The ability to manipulate skyrmions using external pressure offers valuable insights that could enhance their functionality [149, 190]. This suggests the potential to shift the stable skyrmion temperature regime closer to room temperature, or even to higher temperatures,

highlighting the need for a comprehensive pressure-dependent structural investigation of the PtMnGa system.

1.8 Objective of present thesis

The $Ni_2Mn_{1.4}In_{0.6}$ MSMA, among other Ni-Mn-In-based alloys, is significant due to its remarkable technological properties. These include the giant barocaloric effect [154], reversible MCE [156, 191], elastocaloric effect [155], superelastic stability [192], colossal negative magnetoresistance [157], AHE, THE, Nernst effects [157], large exchange bias [158], and the zero-field skyrmionic phase [164], etc. These important technological properties of $Ni_2Mn_{1.4}In_{0.6}$ and related compositions are intricately connected to the magnetostructural transition between the austenite and martensite phases [154, 155, 191, 193]. Although the crystal structure of the martensite phase has been primarily established as 3M modulated [163, 194], the magnetic structure in the so-called PM gap is yet to be fully understood and remains a subject of ongoing debate [163, 195]. Neutron diffraction is a powerful and non-destructive technique that provides detailed insights into the magnetic structure of materials. It has proven to be especially useful in studying the magnetic properties of Ni-Mn-based MSMAs, which exhibit complex structural transitions, particularly in the martensite phase. These materials typically display tetragonal or orthorhombic crystal structures, and neutron diffraction allows to probe the arrangements of magnetic moments within these structures at the atomic level [196–199]. However, neutron diffraction measurements have struggled to fully resolve the magnetic structure of the so-called PM gap in the martensite phase of $Ni_2Mn_{1.4}In_{0.6}$, primarily due to its complex modulated crystal structure [195]. Despite this difficulty, some studies have reported evidence suggesting an antiferromagnetic arrangement of Mn spins at lower temperatures [163]. Recently, the μSR technique has emerged as a highly effective method for probing complex magnetic structures [200–202]. It has also been successfully applied to the study of Ni-Mn-based MSMAs [199, 203], offering valuable insights into their magnetic properties. Our objective is to determine the magnetic state in the so-called PM gap in the martensite phase of the $Ni_2Mn_{1.4}In_{0.6}$ MSMA.

Extensive research has been conducted on Ni-Mn-In-based MSMAs with the goal of using them as suitable materials for magnetic refrigeration applications [60, 192, 204, 205]. The substantial MCE observed in these materials is primarily associated with their first-order magnetostructural (martensite) phase transition (FOMST). However, this same FOMST, which is responsible for the large MCE, also leads to the irreversibility of the phase transition under repeated magnetic field cycles, posing a significant challenge for the development of magnetic refrigeration devices [60, 204, 206]. The irreversibility observed in these materials is linked to the thermal hysteresis of the FOMST, which arises from significant stress at the transition layer between the austenite and martensite phases. In recent years, there has been increased focus within the scientific community on minimizing this hysteresis [60, 207–209]. Hysteresis is an inherent characteristic of materials undergoing FOMST. One approach to reducing hysteresis is by substituting atoms at specific atomic sites [210, 211]. Comparing the MCE of different Ni-Mn-In-based MSMAs it turns out that $Ni_2Mn_{1.4}In_{0.6}$ is one of the best composition for the MCE application due to its large ΔS_{iso} and ΔT_{ad}. However, its large thermal hysteresis ($\sim$ 8 K) leads to irreversibility under repeated magnetic field cycles, posing a significant challenge. This study aims to address this issue by substituting Pt in place of Ni to reduce hysteresis and evaluate the reversibility of the system. The reversibility will be assessed indirectly by calculating ΔS_{iso} from magnetization data obtained under three different measurement protocols. Additionally, the middle eigenvalue of the transformation matrix will be computed to verify the crystallographic compatibility condition.

MCE in magnetocaloric materials is characterized by two key parameters: ΔS_{iso} and ΔT_{ad}. ΔS_{iso} can be determined through isothermal magnetization measurements as a function of the magnetic field. When combined with temperature- and field-dependent heat capacity (C) measurements, ΔS_{iso} can also be used to estimate the ΔT_{ad}. This approach represents an indirect method for evaluating the MCE. This method is well-established, with magnetization and heat capacity measurement instruments being widely accessible. Consequently, indirect evaluations of the MCE are frequently reported. Pecharsky et al. analyzed the error associated with this approach, finding it to be around 15% for pure

Gd. Despite its potential inaccuracies, indirect measurement remains a popular choice due to its practicality and ease of use. To measure ΔT_{ad} directly requires an experimental setup capable of recording temperature changes under adiabatic conditions when the magnetic field is varied. Over the past two decades, numerous prototypes and measurement setups have been developed. However, direct measurements of ΔT_{ad} are less frequently reported in the literature on magnetocaloric materials compared to ΔS_{iso}. This is mainly due to the limited availability of suitable commercial instruments. Our goal is to design a simple experimental setup to measure the direct MCE (ΔT_{ad}).

Typically, Ni-Mn-In-based MSMAs undergo a direct transformation from the austenite phase to the martensite phase during cooling [212]. However, recent studies have shown that some Ni-Mn-In-based MSMAs transition from the austenite (cubic) phase to the martensite (low symmetry) phase via a PM-phase during cooling [164, 172, 172, 213]. Investigation of the magnetotransport properties in the PM-phase of these MSMAs is crucial due to the presence of exotic phenomena like skyrmions. [164, 171, 214, 215]. The PM-phase plays a key role in facilitating the formation of skyrmionic textures in $Ni_2Mn_{1.4}In_{0.6}$ and is closely associated with the twinning and magnetic anisotropy of the system during phase transitions [164]. Generally, the PM-phase exists within a narrow temperature range. However, a recent study suggests that the PM-phase can be stabilized over a broader temperature range through chemical doping [173]. For instance, chemical doping has been reported to stabilize the PM-phase in $Ni_{50}Mn_{34}In_{15.2}Al_{0.8}$ MSMAs in the broad temperature range [173]. Consequently, studying the temperature-dependent magnetotransport properties in the PM-phase is crucial. In the PM-phase, slight lattice distortions and modulated structures amplify the competition between ferromagnetic exchange and antiferromagnetic coupling, providing an ideal environment for non-coplanar spin configurations.

The formation of skyrmions (non-coplanar spin configurations) is well understood in non-centrosymmetric materials due to the presence of DMI [147], but it continues to be a subject of debate in centrosymmetric materials [216, 217]. PtMnGa is known to host Néel skyrmions, which are topologically protected spin structures [186]. Initially, it was as-

sumed that PtMnGa exhibited a hexagonal crystal structure, and it was classified under the centrosymmetric $P6_3/mmc$ space group based on early studies [218]. However, recent studies utilizing single crystal X-ray diffraction and selected-area electron diffraction have suggested a trigonal structure for PtMnGa, with a noncentrosymmetric $P3m1$ space group [186]. This helps to explain the formation of Néel-type skyrmions in PtMnGa [186]. More recent studies on the average structure of PtMnGa using synchrotron X-ray diffraction and neutron powder diffraction have found no evidence supporting the $P3m1$ space group [219]. However, selected-area electron diffraction may offer valuable insights at the local scale [220]. It has been suggested that the local structure of PtMnGa follows the $P3m1$ symmetry. The presence of skyrmions can be explained by local symmetry breaking or structural disorder, even in the absence of long-range ordering in crystalline materials [221]. PtMnGa exhibits thermodynamically stable bulk-type Néel skyrmions within the temperature range of 210–220 K. Achieving stable skyrmions near room temperature is highly desirable for technological applications. Notably, in the PtMnGa system, T_C increases with hydrostatic pressure at a rate of $dT_C/dP = 1.7$ K/kbar. This indicates the potential to shift the stable skyrmion temperature regime (210–220 K) closer to or even beyond room temperature. Therefore, a detailed pressure-dependent structural investigation of the PtMnGa system is essential. Our objective is to tune the skyrmion stability regime through the application of external hydrostatic pressure. The ultimate aim is to bring this regime closer to room temperature, making it more suitable for practical applications.

References

[1] K. Ullakko, "Magnetically controlled shape memory alloys: A new class of actuator materials," *J. Mater. Eng. Perform.*, vol. 5, pp. 405–409, 1996.

[2] K. Ullakko, J. Huang, C. Kantner, R. O'handley, and V. Kokorin, "Large magnetic-field-induced strains in Ni_2MnGa single crystals," *Appl. Phys. Lett.*, vol. 69, no. 13, pp. 1966–1968, 1996.

[3] A. Sozinov, A. Likhachev, N. Lanska, and K. Ullakko, "Giant magnetic-field-induced strain in NiMnGa seven-layered martensitic phase," *Appl. Phys. Lett.*, vol. 80, no. 10, pp. 1746–1748, 2002.

[4] S. J. Murray, M. Marioni, S. Allen, R. O'handley, and T. A. Lograsso, "6% magnetic-field-induced strain by twin-boundary motion in ferromagnetic Ni-Mn-Ga," *Appl. Phys. Lett.*, vol. 77, no. 6, pp. 886–888, 2000.

[5] X. Moya, E. Defay, V. Heine, and N. D. Mathur, "Too cool to work," *Nat. Phys.*, vol. 11, no. 3, pp. 202–205, 2015.

[6] C. Biswas, R. Rawat, and S. Barman, "Large negative magnetoresistance in a ferromagnetic shape memory alloy: $Ni_{2+x}Mn_{1-x}Ga$," *Appl. Phys. Lett.*, vol. 86, no. 20, 2005.

[7] Y. Kuo, K. Sivakumar, H. Chen, J. Su, and C.-S. Lue, "Anomalous thermal properties of the Heusler alloy $Ni_{2+x}Mn_{1-x}Ga$ near the martensitic transition," *Phys. Rev. B*, vol. 72, no. 5, p. 054116, 2005.

[8] Z. Han, B. Qian, D. Wang, P. Zhang, X. Jiang, C. Zhang, and Y. Du, "Magnetic phase separation and exchange bias in off-stoichiometric Ni-Mn-Ga alloys," *Appl. Phys. Lett.*, vol. 103, no. 17, 2013.

[9] S. Chatterjee, S. Giri, S. De, and S. Majumdar, "Reentrant-spin-glass state in $Ni_2Mn_{1.36}Sn_{0.64}$ shape-memory alloy," *Phys. Rev. B*, vol. 79, no. 9, p. 092410, 2009.

[10] R. Nevgi and K. Priolkar, "Unusual strain glassy phase in Fe doped $Ni_2Mn_{1.5}In_{0.5}$," *Appl. Phys. Lett.*, vol. 112, no. 2, 2018.

[11] C. Phatak, O. Heinonen, M. De Graef, and A. Petford-Long, "Nanoscale skyrmions in a nonchiral metallic multiferroic: Ni_2MnGa," *Nano Lett.*, vol. 16, no. 7, pp. 4141–4148, 2016.

[12] I. Dubenko, A. Pathak, S. Stadler, N. Ali, Y. Kovarskii, V. Prudnikov, N. Perov, and A. Granovsky, "Giant Hall effect in Ni-Mn-In Heusler alloys," *Phys. Rev. B*, vol. 80, no. 9, p. 092408, 2009.

[13] A. De, A. K. Singh, S. Singh, and S. Nair, "Temperature dependence of the anomalous Nernst effect in Ni_2MnGa shape memory alloy," *Phys. Rev. B*, vol. 103, no. 2, p. L020404, 2021.

[14] A. Ölander, "An electrochemical investigation of solid cadmium-gold alloys," *J. Am. Chem. Soc.*, vol. 54, no. 10, pp. 3819–3833, 1932.

[15] L. B. Vernon and H. M. Vernon, "Process of manufacturing articles of thermoplastic synthetic resins," Mar. 18 1941. US Patent 2,234,993.

[16] W. J. Buehler, J. V. Gilfrich, and R. Wiley, "Effect of low-temperature phase changes on the mechanical properties of alloys near composition TiNi," *J. Appl. Phys.*, vol. 34, no. 5, pp. 1475–1477, 1963.

[17] G. B. Kauffman and I. Mayo, "The story of nitinol: the serendipitous discovery of the memory metal and its applications," *Chem. Educator*, vol. 2, pp. 1–21, 1997.

[18] Y. Furuya, "Design and material evaluation of shape memory composites," *J. Intell. Mater. Syst. Struct.*, vol. 7, no. 3, pp. 321–330, 1996.

[19] D. J. Leo, C. Weddle, G. Naganathan, and S. J. Buckley, "Vehicular applications of smart material systems," in *Smart structures and materials 1998: Industrial and commercial applications of smart structures technologies*, vol. 3326, pp. 106–116, SPIE, 1998.

[20] D. Stoeckel, "Shape memory actuators for automotive applications," *Mater. Des.*, vol. 11, no. 6, pp. 302–307, 1990.

[21] C. Bil, K. Massey, and E. J. Abdullah, "Wing morphing control with shape memory alloy actuators," *J. Intell. Mater. Syst. Struct.*, vol. 24, no. 7, pp. 879–898, 2013.

[22] D. J. Hartl and D. C. Lagoudas, "Aerospace applications of shape memory alloys," *Proc. Inst. Mech. Eng. Pt. G J. Aerosp. Eng.*, vol. 221, no. 4, pp. 535–552, 2007.

[23] J. Van Humbeeck, "Non-medical applications of shape memory alloys," *Mater. Sci. Eng. A.*, vol. 273, pp. 134–148, 1999.

[24] L. M. Schetky, "Shape memory alloy applications in space systems," *Mater. Des.*, vol. 12, no. 1, pp. 29–32, 1991.

[25] L. Sun, W. M. Huang, Z. Ding, Y. Zhao, C. C. Wang, H. Purnawali, and C. Tang, "Stimulus-responsive shape memory materials: a review," *Mater. Des.*, vol. 33, pp. 577–640, 2012.

[26] M. Kohl, *Shape memory microactuators*. Springer Science & Business Media, 2013.

[27] M. M. Kheirikhah, S. Rabiee, and M. E. Edalat, "A review of shape memory alloy actuators in robotics," *RoboCup 2010: Robot Soccer World Cup XIV 14*, pp. 206–217, 2011.

[28] M. Sreekumar, T. Nagarajan, M. Singaperumal, M. Zoppi, and R. Molfino, "Critical review of current trends in shape memory alloy actuators for intelligent robots," *Ind. Robot.*, vol. 34, no. 4, pp. 285–294, 2007.

[29] T. Duerig, A. Pelton, and D. Stöckel, "An overview of nitinol medical applications," *Mater. Sci. Eng. A.*, vol. 273, pp. 149–160, 1999.

[30] L. Machado and M. Savi, "Medical applications of shape memory alloys," *Braz. J. Med. Biol. Res.*, vol. 36, pp. 683–691, 2003.

[31] R. Chaudhari, J. J. Vora, and D. Parikh, "A review on applications of nitinol shape

memory alloy," *Recent Advances in Mechanical Infrastructure: Proceedings of ICRAM 2020*, pp. 123–132, 2021.

[32] J. M. Jani, M. Leary, A. Subic, and M. A. Gibson, "A review of shape memory alloy research, applications and opportunities," *Mater. Des.*, vol. 56, pp. 1078–1113, 2014.

[33] L. Sun and W. Huang, "Nature of the multistage transformation in shape memory alloys upon heating.," *Met Sci Heat Treat.*, vol. 51, 2009.

[34] I. Mihálcz, "Fundamental characteristics and design method for nickel-titanium shape memory alloy," *Period. Polytech. Mech. Eng.*, vol. 45, no. 1, pp. 75–86, 2001.

[35] D. Lagoudas, *Shape Memory Alloys: Modeling and Engineering Applications*. Springer ebook collection / Chemistry and Materials Science 2005-2008, Springer US, 2008.

[36] G. Welsch, R. Boyer, and E. Collings, *Materials properties handbook: titanium alloys*. ASM international, 1993.

[37] J. Perkins and D. Hodgson, "The two-way shape memory effect," *Engineering aspects of shape memory alloys*, pp. 195–206, 1990.

[38] S. Alipour, F. Taromian, E. R. Ghomi, M. Zare, S. Singh, and S. Ramakrishna, "Nitinol: From historical milestones to functional properties and biomedical applications," *Proc. Inst. Mech. Eng. H*, vol. 236, no. 11, pp. 1595–1612, 2022.

[39] J. Ma, I. Karaman, and R. D. Noebe, "High temperature shape memory alloys," *Int. Mater. Rev.*, vol. 55, no. 5, pp. 257–315, 2010.

[40] J. Pons, V. Chernenko, R. Santamarta, and E. Cesari, "Crystal structure of martensitic phases in Ni-Mn-Ga shape memory alloys," *Acta Mater.*, vol. 48, no. 12, pp. 3027–3038, 2000.

[41] A. Dannenberg, *Ab Initio and Monte Carlo Investigations of Structural, Electronic*

and Magnetic Properties of New Ferromagnetic Heusler Alloys with High Curie Temperatures. 2011.

[42] D. A. Porter and K. E. Easterling, *Phase transformations in metals and alloys (revised reprint)*. CRC press, 2009.

[43] H. Bhadeshia, "Martensitic transformation," *Encyclopedia of Materials: Science and Technology*, pp. 5203–5206, 2001.

[44] P. Müllner and A. H. King, "Deformation of hierarchically twinned martensite," *Acta Mater.*, vol. 58, no. 16, pp. 5242–5261, 2010.

[45] Z. Nishiyama, *Martensitic transformation*. Elsevier, 2012.

[46] K. Otsuka and C. M. Wayman, *Shape memory materials*. Cambridge university press, 1999.

[47] S. Kustov, D. Salas, E. Cesari, R. Santamarta, and J. Van Humbeeck, "Isothermal and athermal martensitic transformations in Ni-Ti shape memory alloys," *Acta Mater.*, vol. 60, no. 6-7, pp. 2578–2592, 2012.

[48] P. Tolédano, G. Krexner, M. Prem, H.-P. Weber, and V. Dmitriev, "Theory of the martensitic transformation in cobalt," *Phys. Rev. B*, vol. 64, no. 14, p. 144104, 2001.

[49] W. Petry, A. Heiming, J. Trampenau, M. Alba, C. Herzig, H. Schober, and G. Vogl, "Phonon dispersion of the bcc phase of group-IV metals. I. bcc titanium," *Phys. Rev. B*, vol. 43, no. 13, p. 10933, 1991.

[50] J. Tellinen, I. Suorsa, A. Jääskeläinen, I. Aaltio, and K. Ullakko, "Basic properties of magnetic shape memory actuators," in *8th international conference ACTUATOR*, vol. 2002, pp. 10–12, 2002.

[51] S. Rashidi, M. H. Ehsani, M. Shakouri, and N. Karimi, "Potentials of magnetic shape memory alloys for energy harvesting," *J. Magn. Magn. Mater.*, vol. 537, p. 168112, 2021.

[52] K. Tsuchiya, A. Tsutsumi, H. Ohtsuka, and M. Umemoto, "Modification of Ni-Mn-

Ga ferromagnetic shape memory alloy by addition of rare earth elements," *Mater. Sci. Eng. A.*, vol. 378, no. 1-2, pp. 370–376, 2004.

[53] O. Heczko and L. Straka, "Temperature dependence and temperature limits of magnetic shape memory effect," *J. Appl. Phys.*, vol. 94, no. 11, pp. 7139–7143, 2003.

[54] H. E. Karaca, I. Karaman, B. Basaran, Y. Ren, Y. I. Chumlyakov, and H. J. Maier, "Magnetic Field-Induced Phase Transformation in NiMnCoIn Magnetic Shape-Memory Alloys—A New Actuation Mechanism with Large Work Output," *Adv. Funct. Mater.*, vol. 19, no. 7, pp. 983–998, 2009.

[55] C. P. Henry, *Dynamic actuation properties of Ni-Mn-Ga ferromagnetic shape memory alloys*. PhD thesis, Massachusetts Institute of Technology, 2002.

[56] F. Heusler, W. Starck, and E. Haupt, "Magnetisch-chemische studien," *Verh. Dtsch. Phys. Ges*, vol. 5, pp. 219–232, 1903.

[57] T. Graf, C. Felser, and S. S. Parkin, "Simple rules for the understanding of Heusler compounds," *Prog. Solid State Chem.*, vol. 39, no. 1, pp. 1–50, 2011.

[58] S. V. Faleev, Y. Ferrante, J. Jeong, M. G. Samant, B. Jones, and S. S. Parkin, "Unified explanation of chemical ordering, the Slater-pauling rule, and half-metallicity in full Heusler compounds," *Phys. Rev. B*, vol. 95, no. 4, p. 045140, 2017.

[59] S. Tavares, K. Yang, and M. A. Meyers, "Heusler alloys: Past, properties, new alloys, and prospects," *Prog. Mater. Sci.*, vol. 132, p. 101017, 2023.

[60] J. Liu, T. Gottschall, K. P. Skokov, J. D. Moore, and O. Gutfleisch, "Giant magnetocaloric effect driven by structural transitions," *Nat. Mater.*, vol. 11, no. 7, pp. 620–626, 2012.

[61] S. Singh, P. Kushwaha, F. Scheibel, H.-P. Liermann, S. Barman, M. Acet, C. Felser, and D. Pandey, "Residual stress induced stabilization of martensite phase and its effect on the magnetostructural transition in Mn-rich Ni-Mn-In/Ga magnetic shape-memory alloys," *Phys. Rev. B*, vol. 92, no. 2, p. 020105, 2015.

[62] S. Singh, R. Rawat, S. E. Muthu, S. D'Souza, E. Suard, A. Senyshyn, S. Banik, P. Rajput, S. Bhardwaj, A. Awasthi, *et al.*, "Spin-valve-like magnetoresistance in Mn_2NiGa at room temperature," *Phys. Rev. Lett.*, vol. 109, no. 24, p. 246601, 2012.

[63] A. K. Nayak, C. Shekhar, J. Winterlik, A. Gupta, and C. Felser, "Mn2PtIn: A tetragonal Heusler compound with exchange bias behavior," *Appl. Phys. Lett.*, vol. 100, no. 15, 2012.

[64] O. Meshcheriakova, S. Chadov, A. Nayak, U. Rößler, J. Kübler, G. André, A. Tsirlin, J. Kiss, S. Hausdorf, A. Kalache, *et al.*, "Large noncollinearity and spin reorientation in the novel Mn_2RhSn Heusler magnet," *Phys. Rev. Lett.*, vol. 113, no. 8, p. 087203, 2014.

[65] A. K. Nayak, M. Nicklas, S. Chadov, C. Shekhar, Y. Skourski, J. Winterlik, and C. Felser, "Large zero-field cooled exchange-bias in bulk Mn_2PtGa," *Phys. Rev. Lett.*, vol. 110, no. 12, p. 127204, 2013.

[66] A. Tishin, K. Gschneidner Jr, and V. Pecharsky, "Magnetocaloric effect and heat capacity in the phase-transition region," *Phys. Rev. B*, vol. 59, no. 1, p. 503, 1999.

[67] P. Weiss and A. Piccard, "Le phénomène magn étocalorique," *J. Phys. Theor. Appl.*, vol. 7, no. 1, pp. 103–109, 1917.

[68] P. Weiss and A. Piccard, "A new thermomagnetic phenomenon," *C. R. Hebd. Seances Acad. Sci*, vol. 166, pp. 352–354, 1918.

[69] P. Debye, "Some observations on magnetisation at a low temperature," *Ann. Physik*, vol. 81, no. 1154-1160, p. 7, 1926.

[70] W. Giauque, "A thermodynamic treatment of certain magnetic effects. a proposed method of producing temperatures considerably below 1 absolute," *J. Am. Chem. Soc.*, vol. 49, no. 8, pp. 1864–1870, 1927.

[71] W. Giauque and D. MacDougall, "Attainment of temperatures below 1 absolute by demagnetization of $Gd_2(SO_4)_3 \cdot 8H_2O$," *Phys. Rev.*, vol. 43, no. 9, p. 768, 1933.

[72] V. K. Pecharsky and K. A. Gschneidner Jr, "Magnetocaloric effect and magnetic refrigeration," *J. Magn. Magn. Mater*, vol. 200, no. 1-3, pp. 44–56, 1999.

[73] K. Gschneidner Jr and V. K. Pecharsky, "Magnetocaloric materials," *Annu. Rev. Mater. Sci.*, vol. 30, no. 1, pp. 387–429, 2000.

[74] C. Zimm, A. Jastrab, A. Sternberg, V. Pecharsky, K. Gschneidner, M. Osborne, and I. Anderson, "Description and performance of a near-room temperature magnetic refrigerator," *Adv. Cryog. Eng.*, pp. 1759–1766, 1998.

[75] V. K. Pecharsky and K. A. Gschneidner Jr, "Giant magnetocaloric effect in $Gd_5(Si_2Ge_2)$," *Phys. Rev. Lett.*, vol. 78, no. 23, p. 4494, 1997.

[76] K. Gschneidner Jr and V. Pecharsky, "Magnetic refrigeration materials," *J. Appl. Phys.*, vol. 85, no. 8, pp. 5365–5368, 1999.

[77] R. Niemann, O. Heczko, L. Schultz, and S. Fähler, "Inapplicability of the Maxwell relation for the quantification of caloric effects in anisotropic ferroic materials," *Int. J. Refrig.*, vol. 37, pp. 281–288, 2014.

[78] I. Takeuchi and K. Sandeman, "Solid-state cooling with caloric materials," *Phys. Today*, vol. 68, no. 12, pp. 48–54, 2015.

[79] A. Smith, C. R. Bahl, R. Bjørk, K. Engelbrecht, K. K. Nielsen, and N. Pryds, "Materials challenges for high performance magnetocaloric refrigeration devices," *Adv. Energy Mater.*, vol. 2, no. 11, pp. 1288–1318, 2012.

[80] S. Y. Dan'Kov, A. Tishin, V. Pecharsky, K. Gschneidner, *et al.*, "Magnetic phase transitions and the magnetothermal properties of gadolinium," *Phys. Rev. B*, vol. 57, no. 6, p. 3478, 1998.

[81] H. Wada and Y. Tanabe, "Giant magnetocaloric effect of $MnAs_{1-x}Sb_x$," *Appl. Phys. Lett.*, vol. 79, no. 20, pp. 3302–3304, 2001.

[82] M. Pasquale, C. P. Sasso, L. Lewis, L. Giudici, T. Lograsso, and D. Schlagel,

"Magnetostructural transition and magnetocaloric effect in $Ni_{55}Mn_{20}Ga_{25}$ single crystals," *Phys. Rev. B*, vol. 72, no. 9, p. 094435, 2005.

[83] T. Krenke, E. Duman, M. Acet, E. F. Wassermann, X. Moya, L. Mañosa, and A. Planes, "Inverse magnetocaloric effect in ferromagnetic Ni-Mn-Sn alloys," *Nat. Mater.*, vol. 4, no. 6, pp. 450–454, 2005.

[84] S. Nikitin, G. Myalikgulyev, A. Tishin, M. Annaorazov, K. Asatryan, and A. Tyurin, "The magnetocaloric effect in $Fe_{49}Rh_{51}$ compound," *Phys. Lett. A*, vol. 148, no. 6-7, pp. 363–366, 1990.

[85] B. Ponomarev, "Magnetic properties of gadolinium in the region of paraprocess," *J. Magn. Magn. Mater.*, vol. 61, no. 1-2, pp. 129–138, 1986.

[86] S. Y. Dan'kov, A. Tishin, V. Pecharsky, and K. Gschneidner, "Experimental device for studying the magnetocaloric effect in pulse magnetic fields," *Rev. Sci. Instrum.*, vol. 68, no. 6, pp. 2432–2437, 1997.

[87] B. Gopal, R. Chahine, and T. Bose, "A sample translatory type insert for automated magnetocaloric effect measurements," *Rev. Sci. Instrum.*, vol. 68, no. 4, pp. 1818–1822, 1997.

[88] B. Gopal, R. Chahine, M. Földeàki, and T. Bose, "Noncontact thermoacoustic method to measure the magnetocaloric effect," *Rev. Sci. Instrum.*, vol. 66, no. 1, pp. 232–238, 1995.

[89] X. Moya, S. Kar-Narayan, and N. D. Mathur, "Caloric materials near ferroic phase transitions," *Nat. Mater.*, vol. 13, no. 5, pp. 439–450, 2014.

[90] A. M. Tishin and Y. I. Spichkin, *The magnetocaloric effect and its applications*. CRC Press, 2016.

[91] X. Moya, L. Mañosa, A. Planes, T. Krenke, E. Duman, M. Acet, and E. Wassermann, "Calorimetric study of the inverse magnetocaloric effect in ferromagnetic Ni-Mn-Sn," *J. Magn. Magn. Mater.*, vol. 316, no. 2, pp. e572–e574, 2007.

[92] K. Gschneidner Jr and V. Pecharsky, "Thirty years of near room temperature magnetic cooling: Where we are today and future prospects," *Int. J. Refrig.*, vol. 31, no. 6, pp. 945–961, 2008.

[93] E. Hall, "XXXVIII. on the new action of magnetism on a permanent electric current," *Lond.Edinb.Dubl.Phil.Mag.*, vol. 10, no. 63, pp. 301–328, 1880.

[94] N. Nagaosa, J. Sinova, S. Onoda, A. H. MacDonald, and N. P. Ong, "Anomalous Hall effect," *Rev. Mod. Phys.*, vol. 82, no. 2, pp. 1539–1592, 2010.

[95] H. Weng, R. Yu, X. Hu, X. Dai, and Z. Fang, "Quantum anomalous Hall effect and related topological electronic states," *Adv. Phys.*, vol. 64, no. 3, pp. 227–282, 2015.

[96] E. H. Hall, "XVIII. on the "Rotational Coefficient" in nickel and cobalt," *Lond.Edinb.Dubl.Phil.Mag.*, vol. 12, no. 74, pp. 157–172, 1881.

[97] A. Kundt, "Das Hall'sche phänomen in Eisen, Kobalt und Nickel," *Ann. Phys. (Berlin)*, vol. 285, no. 6, pp. 257–271, 1893.

[98] E. M. Pugh, N. Rostoker, and A. Schindler, "On the Hall effect in ferromagnetics," *Phys. Rev.*, vol. 80, no. 4, p. 688, 1950.

[99] E. M. Pugh and T. Lippert, "Hall emf and intensity of magnetization," *Phys. Rev.*, vol. 42, no. 5, p. 709, 1932.

[100] E. M. Pugh, "Hall effect and the magnetic properties of some ferromagnetic materials," *Phys. Rev.*, vol. 36, no. 9, p. 1503, 1930.

[101] R. Karplus and J. Luttinger, "Hall effect in ferromagnetics," *Phys. Rev.*, vol. 95, no. 5, p. 1154, 1954.

[102] J. Nitta, "Spin–orbit interaction and spintronics," *JSAP Review*, vol. 2023, p. 230102, 2023.

[103] T. Jungwirth, Q. Niu, and A. MacDonald, "Anomalous Hall effect in ferromagnetic semiconductors," *Phys. Rev. Lett.*, vol. 88, no. 20, p. 207208, 2002.

[104] Y. Tian, L. Ye, and X. Jin, "Proper scaling of the anomalous Hall effect," *Phys. Rev. Lett.*, vol. 103, no. 8, p. 087206, 2009.

[105] G. Sundaram and Q. Niu, "Wave-packet dynamics in slowly perturbed crystals: Gradient corrections and Berry-phase effects," *Phys. Rev. B*, vol. 59, no. 23, p. 14915, 1999.

[106] J. Smit, "The spontaneous Hall effect in ferromagnetics I," *Physica*, vol. 21, no. 6-10, pp. 877–887, 1955.

[107] J. Smit, "The spontaneous Hall effect in ferromagnetics II," *Physica*, vol. 24, no. 1-5, pp. 39–51, 1958.

[108] S. Onoda, N. Sugimoto, and N. Nagaosa, "Intrinsic versus extrinsic anomalous Hall effect in ferromagnets," *Phys. Rev. Lett.*, vol. 97, no. 12, p. 126602, 2006.

[109] P. Bruno, V. Dugaev, and M. Taillefumier, "Topological Hall effect and Berry phase in magnetic nanostructures," *Phys. Rev. Lett.*, vol. 93, no. 9, p. 096806, 2004.

[110] S. Sen, C. Singh, P. K. Mukharjee, R. Nath, and A. K. Nayak, "Observation of the topological Hall effect and signature of room-temperature antiskyrmions in Mn-Ni-Ga D_{2d} Heusler magnets," *Phys. Rev. B*, vol. 99, no. 13, p. 134404, 2019.

[111] V. Kumar, N. Kumar, M. Reehuis, J. Gayles, A. Sukhanov, A. Hoser, F. Damay, C. Shekhar, P. Adler, and C. Felser, "Detection of antiskyrmions by topological Hall effect in Heusler compounds," *Phys. Rev. B*, vol. 101, no. 1, p. 014424, 2020.

[112] A. Neubauer, C. Pfleiderer, B. Binz, A. Rosch, R. Ritz, P. Niklowitz, and P. Böni, "Topological Hall effect in the A phase of MnSi," *Phys. Rev. Lett.*, vol. 102, no. 18, p. 186602, 2009.

[113] T. Moriya, "Anisotropic superexchange interaction and weak ferromagnetism," *Phys. Rev.*, vol. 120, no. 1, p. 91, 1960.

[114] I. Dzyaloshinsky, "A thermodynamic theory of "weak" ferromagnetism of antiferromagnetics," *J. Phys. Chem. Solids.*, vol. 4, no. 4, pp. 241–255, 1958.

[115] U. K. Roessler, A. Bogdanov, and C. Pfleiderer, "Spontaneous skyrmion ground states in magnetic metals," *Nat.*, vol. 442, no. 7104, pp. 797–801, 2006.

[116] Y. Taguchi, Y. Oohara, H. Yoshizawa, N. Nagaosa, and Y. Tokura, "Spin chirality, Berry phase, and anomalous Hall effect in a frustrated ferromagnet," *Sci.*, vol. 291, no. 5513, pp. 2573–2576, 2001.

[117] N. Kanazawa, Y. Onose, T. Arima, D. Okuyama, K. Ohoyama, S. Wakimoto, K. Kakurai, S. Ishiwata, and Y. Tokura, "Large topological Hall effect in a short-period helimagnet MnGe," *Phys. Rev. Lett.*, vol. 106, no. 15, p. 156603, 2011.

[118] M. Onoda, G. Tatara, and N. Nagaosa, "Anomalous Hall effect and skyrmion number in real and momentum spaces," *J. Phys. Soc. Jpn.* ., vol. 73, no. 10, pp. 2624–2627, 2004.

[119] N. Nagaosa, "Anomalous Hall effect—a new perspective—," *J. Phys. Soc. Jpn.* ., vol. 75, no. 4, pp. 042001–042001, 2006.

[120] P. Bruno, V. Dugaev, and M. Taillefumier, "Topological Hall effect in magnetic nanostructures," *Phys. Rev. Lett*, vol. 93, pp. 58–59, 2012.

[121] F. Freimuth, R. Bamler, Y. Mokrousov, and A. Rosch, "Phase-space Berry phases in chiral magnets: Dzyaloshinskii-Moriya interaction and the charge of skyrmions," *Phys. Rev. B*, vol. 88, no. 21, p. 214409, 2013.

[122] C. Franz, F. Freimuth, A. Bauer, R. Ritz, C. Schnarr, C. Duvinage, T. Adams, S. Blügel, A. Rosch, Y. Mokrousov, *et al.*, "Real-space and reciprocal-space Berry phases in the Hall effect of $Mn_{1-x}Fe_xSi$," *Phys. Rev. Lett.*, vol. 112, no. 18, p. 186601, 2014.

[123] G. Tatara, H. Kohno, J. Shibata, Y. Lemaho, and K.-J. Lee, "Spin torque and force due to current for general spin textures," *J. Phys. Soc. Jpn.* ., vol. 76, no. 5, pp. 054707–054707, 2007.

[124] A. Fert, N. Reyren, and V. Cros, "Magnetic skyrmions: advances in physics and potential applications," *Nat. Rev. Mater.*, vol. 2, no. 7, pp. 1–15, 2017.

[125] T. Skyrme, "A unified model of K-and π-mesons," *Proc. R. soc. Lond. Ser. A*, vol. 252, no. 1269, pp. 236–245, 1959.

[126] T. Skyrme, "A unified model of K-and π-mesons," in *Selected Papers, With Commentary, Of Tony Hilton Royle Skyrme*, pp. 185–194, World Scientific, 1994.

[127] T. H. R. Skyrme, "A unified field theory of mesons and baryons," *Nucl. Phys.*, vol. 31, pp. 556–569, 1962.

[128] S. Mühlbauer, B. Binz, F. Jonietz, C. Pfleiderer, A. Rosch, A. Neubauer, R. Georgii, and P. Böni, "Skyrmion lattice in a chiral magnet," *Sci.*, vol. 323, no. 5916, pp. 915–919, 2009.

[129] Y. Tokura and N. Kanazawa, "Magnetic skyrmion materials," *Chem. Rev.*, vol. 121, no. 5, pp. 2857–2897, 2020.

[130] A. K. Nayak, V. Kumar, T. Ma, P. Werner, E. Pippel, R. Sahoo, F. Damay, U. K. Rößler, C. Felser, and S. S. Parkin, "Magnetic antiskyrmions above room temperature in tetragonal Heusler materials," *Nat.*, vol. 548, no. 7669, pp. 561–566, 2017.

[131] S. Wang, J. Tang, W. Wang, L. Kong, M. Tian, and H. Du, "Electrical detection of magnetic skyrmions," *J. Low Temp. Phys.*, vol. 197, pp. 321–336, 2019.

[132] E. Y. Tsymbal and C. Panagopoulos, "Whirling spins with a ferroelectric," *Nat. Mater.*, vol. 17, no. 12, pp. 1054–1055, 2018.

[133] K. Shibata, X. Yu, T. Hara, D. Morikawa, N. Kanazawa, K. Kimoto, S. Ishiwata, Y. Matsui, and Y. Tokura, "Towards control of the size and helicity of skyrmions in helimagnetic alloys by spin-orbit coupling," *Nat. Nanotechnol.*, vol. 8, no. 10, pp. 723–728, 2013.

[134] B. Lebech, J. Bernhard, and T. Freltoft, "Magnetic structures of cubic FeGe studied by small-angle neutron scattering," *J. Condens. Matter Phys.*, vol. 1, no. 35, p. 6105, 1989.

[135] X. Yu, N. Kanazawa, Y. Onose, K. Kimoto, W. Zhang, S. Ishiwata, Y. Matsui, and

Y. Tokura, "Near room-temperature formation of a skyrmion crystal in thin-films of the helimagnet FeGe," *Nat. Mater.*, vol. 10, no. 2, pp. 106–109, 2011.

[136] S. Seki, X. Yu, S. Ishiwata, and Y. Tokura, "Observation of skyrmions in a multiferroic material," *Sci.*, vol. 336, no. 6078, pp. 198–201, 2012.

[137] T. Adams, A. Chacon, M. Wagner, A. Bauer, G. Brandl, B. Pedersen, H. Berger, P. Lemmens, and C. Pfleiderer, "Long-wavelength helimagnetic order and skyrmion lattice phase in Cu_2OSeO_3," *Phys. Rev. Lett.*, vol. 108, no. 23, p. 237204, 2012.

[138] K. Karube, K. Shibata, J. White, T. Koretsune, X. Yu, Y. Tokunaga, H. Rønnow, R. Arita, T. Arima, Y. Tokura, *et al.*, "Controlling the helicity of magnetic skyrmions in a β-Mn-type high-temperature chiral magnet," *Phys. Rev. B*, vol. 98, no. 15, p. 155120, 2018.

[139] S. Heinze, K. Von Bergmann, M. Menzel, J. Brede, A. Kubetzka, R. Wiesendanger, G. Bihlmayer, and S. Blügel, "Spontaneous atomic-scale magnetic skyrmion lattice in two dimensions," *Nat. Phys.*, vol. 7, no. 9, pp. 713–718, 2011.

[140] J. C. Loudon, A. C. Twitchett-Harrison, D. Cortés-Ortuño, M. T. Birch, L. A. Turnbull, A. Štefančič, F. Y. Ogrin, E. O. Burgos-Parra, N. Bukin, A. Laurenson, *et al.*, "Do images of Biskyrmions show type-II bubbles?," *Adv. Mater.*, vol. 31, no. 16, p. 1806598, 2019.

[141] B. Ding, J. Cui, G. Xu, Z. Hou, H. Li, E. Liu, G. Wu, Y. Yao, and W. Wang, "Manipulating spin chirality of magnetic skyrmion bubbles by in-plane reversed magnetic fields in $(Mn_{1-x}Ni_x)_{65}Ga_{35}$ $(x = 0.45)$ magnet," *Phys. Rev. Appl.*, vol. 12, no. 5, p. 054060, 2019.

[142] L. Kong, J. Tang, W. Wang, Y. Wu, J. Jiang, Y. Wang, J. Li, Y. Xiong, M. Tian, and H. Du, "Observation of hybrid magnetic skyrmion bubbles in Fe_3Sn_2 nanodisks," *Phys. Rev. B*, vol. 107, no. 17, p. 174425, 2023.

[143] M. Altthaler, E. Lysne, E. Roede, L. Prodan, V. Tsurkan, M. A. Kassem, H. Naka-

mura, S. Krohns, I. Kézsmárki, and D. Meier, "Magnetic and geometric control of spin textures in the itinerant kagome magnet Fe_3Sn_2," *Phys. Rev. Res.*, vol. 3, no. 4, p. 043191, 2021.

[144] D. Chakrabartty, S. Jamaluddin, S. K. Manna, and A. K. Nayak, "Tunable room temperature magnetic skyrmions in centrosymmetric kagome magnet Mn_4Ga_2Sn," *Commun. Phys.*, vol. 5, no. 1, p. 189, 2022.

[145] X. Yu, Y. Tokunaga, Y. Taguchi, and Y. Tokura, "Variation of Topology in Magnetic Bubbles in a Colossal Magnetoresistive Manganite.," *Adv. Mater.*, vol. 29, no. 3, 2016.

[146] B. Ding, Z. Li, G. Xu, H. Li, Z. Hou, E. Liu, X. Xi, F. Xu, Y. Yao, and W. Wang, "Observation of magnetic skyrmion bubbles in a van der Waals ferromagnet Fe_3GeTe_2," *Nano Lett.*, vol. 20, no. 2, pp. 868–873, 2019.

[147] N. Nagaosa and Y. Tokura, "Topological properties and dynamics of magnetic skyrmions," *Nat. Nanotechnol.*, vol. 8, no. 12, pp. 899–911, 2013.

[148] F. Jonietz, S. Mühlbauer, C. Pfleiderer, A. Neubauer, W. Münzer, A. Bauer, T. Adams, R. Georgii, P. Böni, R. A. Duine, *et al.*, "Spin transfer torques in MnSi at ultralow current densities," *Sci.*, vol. 330, no. 6011, pp. 1648–1651, 2010.

[149] K. Shibata, J. Iwasaki, N. Kanazawa, S. Aizawa, T. Tanigaki, M. Shirai, T. Nakajima, M. Kubota, M. Kawasaki, H. Park, *et al.*, "Large anisotropic deformation of skyrmions in strained crystal," *Nat. Nanotechnol.*, vol. 10, no. 7, pp. 589–592, 2015.

[150] L. Kong and J. Zang, "Dynamics of an insulating skyrmion under a temperature gradient," *Phys. Rev. Lett.*, vol. 111, no. 6, p. 067203, 2013.

[151] A. Fert, V. Cros, and J. Sampaio, "Skyrmions on the track," *Nat. Nanotechnol.*, vol. 8, no. 3, pp. 152–156, 2013.

[152] J. Iwasaki, M. Mochizuki, and N. Nagaosa, "Current-induced skyrmion dynamics in constricted geometries," *Nat. Nanotechnol.*, vol. 8, no. 10, pp. 742–747, 2013.

[153] J. Sampaio, V. Cros, S. Rohart, A. Thiaville, and A. Fert, "Nucleation, stability and current-induced motion of isolated magnetic skyrmions in nanostructures," *Nat. Nanotechnol.*, vol. 8, no. 11, pp. 839–844, 2013.

[154] L. Mañosa, D. González-Alonso, A. Planes, E. Bonnot, M. Barrio, J.-L. Tamarit, S. Aksoy, and M. Acet, "Giant solid-state barocaloric effect in the Ni-Mn-In magnetic shape-memory alloy," *Nat. Mater.*, vol. 9, no. 6, pp. 478–481, 2010.

[155] B. Lu and J. Liu, "Elastocaloric effect and superelastic stability in Ni-Mn-In-Co polycrystalline Heusler alloys: hysteresis and strain-rate effects," *Sci. Rep.*, vol. 7, no. 1, pp. 1–11, 2017.

[156] F. Liu, Q. Wang, W. Ao, Y. Yu, L. Pan, and J. Li, "Magnetocaloric effect in high Ni content $Ni_{52}Mn_{48-x}In_x$ alloys under low field change," *J. Magn. Magn. Mater.*, vol. 324, no. 4, pp. 514–518, 2012.

[157] P. Yanda, L. Noohinejad, N. Mao, N. Peshcherenko, K. Imasato, A. K. Srivastava, Y. Guan, B. Giri, A. K. Sharma, K. Manna, *et al.*, "Giant Topological Hall Effect and Colossal Magnetoresistance in Heusler Ferromagnet near Room Temperature," *Adv. Mater.*, p. 2411240, 2024.

[158] B. Wang, Y. Liu, P. Ren, B. Xia, K. Ruan, J. Yi, J. Ding, X. Li, and L. Wang, "Large exchange bias after zero-field cooling from an unmagnetized state," *Phys. Rev. Lett.*, vol. 106, no. 7, p. 077203, 2011.

[159] R. A. Ahamed Khan, R. Ghomashchi, Z. Xie, and L. Chen, "Ferromagnetic shape memory Heusler materials: Synthesis, microstructure characterization and magnetostructural properties," *Materials*, vol. 11, no. 6, p. 988, 2018.

[160] R. Nevgi, K. Priolkar, and L. Righi, "Investigation of route to martensitic transition in Ni-Mn-In shape memory alloys," in *AIP Conf. Proc.*, vol. 1942, AIP Publishing, 2018.

[161] T. Krenke, M. Acet, E. F. Wassermann, X. Moya, L. Mañosa, and A. Planes, "Fer-

romagnetism in the austenitic and martensitic states of Ni-Mn-In alloys," *Phys. Rev. B*, vol. 73, no. 17, p. 174413, 2006.

[162] M. Acet, L. Mañosa, and A. Planes, "Magnetic-field-induced effects in martensitic Heusler-based magnetic shape memory alloys," in *Handb. Magn. Mater.*, vol. 19, pp. 231–289, Elsevier, 2011.

[163] P. Devi, S. Singh, B. Dutta, K. Manna, S. W. D'Souza, Y. Ikeda, E. Suard, V. Petricek, P. Simon, P. Werner, *et al.*, "Adaptive modulation in the $Ni_2Mn_{1.4}In_{0.6}$ magnetic shape-memory Heusler alloy," *Phys. Rev. B*, vol. 97, no. 22, p. 224102, 2018.

[164] S. Zuo, F. Liang, Y. Zhang, L. Peng, J. Xiong, Y. Liu, R. Li, T. Zhao, J. Sun, F. Hu, *et al.*, "Zero-field skyrmions generated via premartensitic transition in $Ni_{50}Mn_{35.2}In_{14.8}$ alloy," *Phys. Rev. Mater.*, vol. 2, no. 10, p. 104408, 2018.

[165] S. Shapiro, J. Larese, Y. Noda, S. Moss, and L. Tanner, "Neutron scattering study of premartensitic behavior in Ni-Al alloys," *Phys. Rev. Lett.*, vol. 57, no. 25, p. 3199, 1986.

[166] G. Sandrock, A. Perkins, and R. Hehemann, "The premartensitic instability in near-equiatomic TiNi," *Metallurgical Transactions*, vol. 2, pp. 2769–2781, 1971.

[167] M. Salamon, M. Meichle, and C. Wayman, "Premartensitic phases of $Ti_{50}Ni_{47}Fe_3$," *Phys. Rev. B*, vol. 31, no. 11, p. 7306, 1985.

[168] L. Manosa, J. Zarestky, T. Lograsso, D. W. Delaney, and C. Stassis, "Lattice-dynamical study of the premartensitic state of the Cu-Al-Be alloys," *Phys. Rev. B*, vol. 48, no. 21, p. 15708, 1993.

[169] M. Blinov, V. Chernenko, V. Prudnikov, I. Aseguinolaza, J. Barandiaran, E. Lahderanta, and A. Granovsky, "Anomalous Hall effect in $Ni_{47.3}Mn_{30.6}Ga_{22.1}/MgO(001)$ thin films," *Phys. Rev. B*, vol. 102, no. 6, p. 064413, 2020.

[170] F. Li, F. Chen, M. Zhang, K. Zhang, W. Liu, D. Zhao, and B. Yang, "Anomalous Hall effect in epitaxial Ni-Mn-Ga thin films grown on MgO (001) substrate during

the martensitic transformation," *J. Supercond. Nov. Magn.*, vol. 32, pp. 3183–3189, 2019.

[171] A. K. Singh, G. K. Shukla, and S. Singh, "Intrinsic anomalous Hall conductivity and real space Berry curvature induced topological Hall effect in Ni_2MnGa magnetic shape memory alloy," *J. Phys. D Appl. Phys.*, vol. 56, no. 4, p. 044004, 2022.

[172] Y. Wu, S. Guo, S. Yu, H. Cheng, R. Wang, H. Xiao, L. Xu, R. Xiong, Y. Liu, Z. Xia, *et al.*, "Premartensitic transition and relevant magnetic effects in $Ni_{50}Mn_{34}In_{15.5}Al_{0.5}$ alloy," *Sci. Rep.*, vol. 6, no. 1, p. 26068, 2016.

[173] A. K. Singh, S. Singh, B. Dutta, K. Dubey, B. Joseph, R. Rawat, and D. Pandey, "Robust evidence for the stabilization of the premartensite phase in Ni-Mn-In magnetic shape memory alloys by chemical pressure," *Phys. Rev. Mater.*, vol. 5, no. 11, p. 113607, 2021.

[174] E. Liu, W. Wang, L. Feng, W. Zhu, G. Li, J. Chen, H. Zhang, G. Wu, C. Jiang, H. Xu, *et al.*, "Stable magnetostructural coupling with tunable magnetoresponsive effects in hexagonal ferromagnets," *Nat. commun.*, vol. 3, no. 1, p. 873, 2012.

[175] K. Koyama, M. Sakai, T. Kanomata, and K. Watanabe, "Field-induced martensitic transformation in new ferromagnetic shape memory compound $Mn_{1.07}Co_{0.92}Ge$," *Jpn. J. Appl. Phys.*, vol. 43, no. 12R, p. 8036, 2004.

[176] K. Buschow and P. van Engen, "Note on the magnetic and magneto-optical properties of Ni_2In type 3d transition metal compounds," *Phys. Status Solidi A.*, vol. 76, no. 2, pp. 615–620, 1983.

[177] C. Zhang, Z. Han, B. Qian, H. Shi, C. Zhu, J. Chen, and T. Wang, "Magnetostructural transformation and magnetocaloric effect in $MnNiGe_{1-x}Ga_x$ alloys," *J. Appl. Phys.*, vol. 114, no. 15, 2013.

[178] K. Xu, Z. Li, E. Liu, H. Zhou, Y. Zhang, and C. Jing, "Magnetocaloric effect and negative thermal expansion in hexagonal Fe doped MnNiGe compounds with a magnetoelastic AFM-FM-like transition," *Sci. Rep.*, vol. 7, no. 1, p. 41675, 2017.

[179] C. Zhang, D. Wang, Q. Cao, Z. Han, H. Xuan, and Y. Du, "Magnetostructural phase transition and magnetocaloric effect in off-stoichiometric $Mn_{1.9-x}Ni_xGe$ alloys," *Appl. Phys. Lett.*, vol. 93, no. 12, 2008.

[180] P. Dutta, S. Pramanick, V. Singh, D. T. Major, D. Das, and S. Chatterjee, "Anomalous magnetotransport behavior in Fe-doped MnNiGe alloys," *Phys. Rev. B*, vol. 93, no. 13, p. 134408, 2016.

[181] S. Nizioł, A. Bombik, W. Bazela, A. Szytuła, and D. Fruchart, "Crystal and magnetic structure of $Co_xNi_{1-x}MnGe$ system," *J. Magn. Magn. Mater.*, vol. 27, no. 3, pp. 281–292, 1982.

[182] X. Miao, Y. Gong, L. Caron, Y. You, G. Xu, D. Sheptyakov, P. Manuel, F. Qian, Y. Zhang, F. Xu, *et al.*, "Switching the magnetostructural coupling in MnCoGe-based magnetocaloric materials," *Phys. Rev. Mater.*, vol. 4, no. 10, p. 104407, 2020.

[183] C. Zhang, D. Wang, Z. Han, B. Qian, H. Shi, C. Zhu, J. Chen, and T. Wang, "The tunable magnetostructural transition in MnNiSi-FeNiGe system," *Appl. Phys. Lett.*, vol. 103, no. 13, 2013.

[184] J.-T. Wang, D.-S. Wang, C. Chen, O. Nashima, T. Kanomata, H. Mizuseki, and Y. Kawazoe, "Vacancy induced structural and magnetic transition in $MnCo_{1-x}Ge$," *Appl. Phys. Lett.*, vol. 89, no. 26, 2006.

[185] R.-R. Wu, L.-F. Bao, F.-X. Hu, H. Wu, Q.-Z. Huang, J. Wang, X.-L. Dong, G.-N. Li, J.-R. Sun, F.-R. Shen, *et al.*, "Giant barocaloric effect in hexagonal Ni_2In-type Mn-Co-Ge-In compounds around room temperature," *Sci. Rep.*, vol. 5, no. 1, p. 18027, 2015.

[186] A. K. Srivastava, P. Devi, A. K. Sharma, T. Ma, H. Deniz, H. L. Meyerheim, C. Felser, and S. S. Parkin, "Observation of robust Néel skyrmions in metallic PtMnGa," *Adv. Mater.*, vol. 32, no. 7, p. 1904327, 2020.

[187] W. Wang, Y. Zhang, G. Xu, L. Peng, B. Ding, Y. Wang, Z. Hou, X. Zhang, X. Li, E. Liu, S. Wang, J. Cai, F. Wang, J. Li, F. Hu, G. Wu, B. Shen, and X.-X. Zhang,

"A centrosymmetric hexagonal magnet with superstable biskyrmion magnetic nanodomains in a wide temperature range of 100–340 k," *Adv. Mater.*, vol. 28, no. 32, pp. 6887–6893, 2016.

[188] J. A. Cooley, J. D. Bocarsly, E. C. Schueller, E. E. Levin, E. E. Rodriguez, A. Huq, S. H. Lapidus, S. D. Wilson, and R. Seshadri, "Evolution of noncollinear magnetism in magnetocaloric MnPtGa," *Phys. Rev. Mater.*, vol. 4, no. 4, p. 044405, 2020.

[189] T. Kanomata, K. Shirakawa, and T. Kaneko, "Effect of hydrostatic pressure on the Curie temperature of the hexagonal compound PtMnGa," *Phys. Status Solidi A.*, vol. 97, no. 2, pp. K149–K152, 1986.

[190] L. J. Bannenberg, R. Sadykov, R. M. Dalgliesh, C. Goodway, D. L. Schlagel, T. A. Lograsso, P. Falus, E. Lelièvre-Berna, A. O. Leonov, and C. Pappas, "Skyrmions and spirals in MnSi under hydrostatic pressure," *Phys. Rev. B*, vol. 100, no. 5, p. 054447, 2019.

[191] J. Liu, X. You, B. Huang, I. Batashev, M. Maschek, Y. Gong, X. Miao, F. Xu, N. van Dijk, and E. Brück, "Reversible low-field magnetocaloric effect in Ni-Mn-In-based Heusler alloys," *Phys. Rev. Mater.*, vol. 3, no. 8, p. 084409, 2019.

[192] T. Krenke, E. Duman, M. Acet, E. F. Wassermann, X. Moya, L. Mañosa, A. Planes, E. Suard, and B. Ouladdiaf, "Magnetic superelasticity and inverse magnetocaloric effect in Ni-Mn-In," *Phys. Rev. B*, vol. 75, no. 10, p. 104414, 2007.

[193] X. Moya, L. Mañosa, A. Planes, S. Aksoy, M. Acet, E. F. Wassermann, and T. Krenke, "Cooling and heating by adiabatic magnetization in the $Ni_{50}Mn_{34}In_{16}$ magnetic shape-memory alloy," *Phys. Rev. B*, vol. 75, no. 18, p. 184412, 2007.

[194] K. K. Dubey, P. Devi, A. K. Singh, and S. Singh, "Improved crystallographic compatibility and magnetocaloric reversibility in Pt substituted $Ni_2Mn_{1.4}In_{0.6}$ magnetic shape memory Heusler alloy," *J. Magn. Magn. Mater.*, vol. 507, p. 166818, 2020.

[195] P. Brown, A. Gandy, R. Kainuma, T. Kanomata, K. Neumann, K. Oikawa, B. Ouladdiaf, A. Sheikh, and K. Ziebeck, "The field and temperature depen-

dence of the magnetic and structural properties of the shape memory compound $Ni_{1.84}Mn_{1.64}In_{0.52}$," *J. Condens. Matter Phys.*, vol. 23, no. 45, p. 456004, 2011.

[196] P. Brown, A. Gandy, K. Ishida, R. Kainuma, T. Kanomata, K. Neumann, K. Oikawa, B. Ouladdiaf, and K. Ziebeck, "The magnetic and structural properties of the magnetic shape memory compound $Ni_2Mn_{1.44}Sn_{0.56}$," *J. Condens. Matter Phys.*, vol. 18, no. 7, p. 2249, 2006.

[197] P. Brown, A. Gandy, K. Ishida, W. Ito, R. Kainuma, T. Kanomata, K. Neumann, K. Oikawa, B. Ouladdiaf, A. Sheikh, *et al.*, "Magnetic and structural properties of the magnetic shape memory compound $Ni_2Mn_{1.48}Sb_{0.52}$," *J. Condens. Matter Phys.*, vol. 22, no. 9, p. 096002, 2010.

[198] F. Orlandi, S. Fabbrici, F. Albertini, P. Manuel, D. Khalyavin, and L. Righi, "Long-range antiferromagnetic interactions in Ni-Co-Mn-Ga metamagnetic Heusler alloys: A two-step ordering studied by neutron diffraction," *Phys. Rev. B*, vol. 94, no. 14, p. 140409, 2016.

[199] J. Sannigrahi, S. Pramanick, S. Chatterjee, J. Lord, D. Khalyavin, A. Hillier, D. Adroja, and S. Majumdar, "Magnetic states of Ni-Mn-Sn based shape memory alloy: a combined muon spin relaxation and neutron diffraction study," *Phys. Rev. B*, vol. 99, no. 22, p. 224401, 2019.

[200] Y. Wei, X. Ma, Z. Feng, D. Adroja, A. Hillier, P. Biswas, A. Senyshyn, A. Hoser, J.-W. Mei, Z. Y. Meng, *et al.*, "Magnetic phase diagram of $Cu_{4-x}Zn_x(OH)_6FBr$ studied by neutron-diffraction and μSR techniques," *Chin. Phys. Lett.*, vol. 37, no. 10, p. 107503, 2020.

[201] C. Bonilla, N. Marcano, J. Herrero-Albillos, A. Maisuradze, L. García, and F. Bartolomé, "μSR study of short-range magnetic order in the paramagnetic regime of $ErCo_2$," *Phys. Rev. B*, vol. 84, no. 18, p. 184425, 2011.

[202] I. Gat-Malureanu, J. Carlo, T. Goko, A. Fukaya, T. Ito, P. Kyriakou, M. Larkin, G. Luke, P. Russo, A. Savici, *et al.*, "Muon spin relaxation and susceptibility

measurements of an itinerant-electron system $Sr_{(1-x)}Ca_xRuO_3$: quantum evolution from ferromagnet to paramagnet," *Phys. Rev. B*, vol. 84, no. 22, p. 224415, 2011.

[203] M. Wilson, T. Hicken, M. Gomilšek, A. Štefančič, G. Balakrishnan, J. Loudon, A. Twitchett-Harrison, F. Pratt, M. Telling, and T. Lancaster, "Spin dynamics in bulk MnNiGa and $Mn_{1.4}Pt_{0.9}Pd_{0.1}Sn$ investigated by muon spin relaxation," *Phys. Rev. B*, vol. 104, no. 13, p. 134414, 2021.

[204] M. Ghorbani Zavareh, C. Salazar Mejía, A. Nayak, Y. Skourski, J. Wosnitza, C. Felser, and M. Nicklas, "Direct measurements of the magnetocaloric effect in pulsed magnetic fields: The example of the Heusler alloy $Ni_{50}Mn_{35}In_{15}$," *Appl. Phys. Lett.*, vol. 106, no. 7, 2015.

[205] S. Singh, L. Caron, S. W. D'Souza, T. Fichtner, G. Porcari, S. Fabbrici, C. Shekhar, S. Chadov, M. Solzi, and C. Felser, "Large Magnetization and Reversible Magnetocaloric Effect at the Second-Order Magnetic Transition in Heusler Materials," *Adv. Mater.*, vol. 28, no. 17, pp. 3321–3325, 2016.

[206] M. Ghahremani, A. Aslani, M. Hosseinnia, L. H. Bennett, and E. Della Torre, "Direct and indirect measurement of the magnetocaloric effect in bulk and nanostructured Ni-Mn-In Heusler alloy," *AIP Adv.*, vol. 8, no. 5, 2018.

[207] J. Ortín and L. Delaey, "Hysteresis in shape-memory alloys," *Int. J. Non-Linear Mech.*, vol. 37, no. 8, pp. 1275–1281, 2002.

[208] K. Li, Y. Li, K. Yu, C. Liu, D. Gibson, A. Leyland, A. Matthews, and Y. Q. Fu, "Crystal size induced reduction in thermal hysteresis of Ni-Ti-Nb shape memory thin films," *Appl. Phys. Lett.*, vol. 108, no. 17, 2016.

[209] E. Stern-Taulats, P. O. Castillo-Villa, L. Mañosa, C. Frontera, S. Pramanick, S. Majumdar, and A. Planes, "Magnetocaloric effect in the low hysteresis Ni-Mn-In metamagnetic shape-memory Heusler alloy," *J. Appl. Phys.*, vol. 115, no. 17, 2014.

[210] S. Singh, S. D'Souza, J. Nayak, L. Caron, E. Suard, S. Chadov, and C. Felser, "Ef-

fect of platinum substitution on the structural and magnetic properties of Ni_2MnGa ferromagnetic shape memory alloy," *Phys. Rev. B*, vol. 93, no. 13, p. 134102, 2016.

[211] J. Pons, E. Cesari, C. Seguí, F. Masdeu, and R. Santamarta, "Ferromagnetic shape memory alloys: alternatives to Ni-Mn-Ga," *Mater. Sci. Eng. A.*, vol. 481, pp. 57–65, 2008.

[212] X. Moya, L. Mañosa, A. Planes, T. Krenke, M. Acet, and E. F. Wassermann, "Martensitic transition and magnetic properties in Ni-Mn-X alloys," *Mater. Sci. Eng. A.*, vol. 438, pp. 911–915, 2006.

[213] S. Ma, H. Xuan, C. Zhang, L. Wang, Q. Cao, D. Wang, and Y. Du, "Investigation of the intermediate phase and magnetocaloric properties in high-pressure annealing Ni-Mn-Co-Sn alloy," *Appl. Phys. Lett.*, vol. 97, no. 5, 2010.

[214] S. Singh, J. Bednarcik, S. Barman, C. Felser, and D. Pandey, "Premartensite to martensite transition and its implications for the origin of modulation in Ni_2MnGa ferromagnetic shape-memory alloy," *Phys. Rev. B*, vol. 92, no. 5, p. 054112, 2015.

[215] A. Gonzalez-Comas, E. Obradó, L. Mañosa, A. Planes, V. Chernenko, B. J. Hattink, and A. Labarta, "Premartensitic and martensitic phase transitions in ferromagnetic Ni_2MnGa," *Phys. Rev. B*, vol. 60, no. 10, p. 7085, 1999.

[216] D. Capic, D. A. Garanin, and E. M. Chudnovsky, "Biskyrmion lattices in centrosymmetric magnetic films," *Phys. Rev. Res.*, vol. 1, no. 3, p. 033011, 2019.

[217] G. Xu, Y. You, J. Tang, H. Zhang, H. Li, X. Miao, Y. Gong, Z. Hou, Z. Cheng, J. Wang, *et al.*, "Simultaneous tuning of magnetocrystalline anisotropy and spin reorientation transition via Cu substitution in Mn-Ni-Ga magnets for nanoscale biskyrmion formation," *Phys. Rev. B*, vol. 100, no. 5, p. 054416, 2019.

[218] K. Buschow and D. De Mooij, "Crystal structure and magnetic properties of PtMnGa and PtMnAl," *J. Less-Common Met.*, vol. 99, no. 1, pp. 125–130, 1984.

[219] K. Oikawa, T. Ota, Y. Imano, T. Omori, R. Kainuma, and K. Ishida, "Phase equi-

libria and phase transformation of Co- Ni- Ga ferromagnetic shape memory alloy system," *J. Ph. Equilibria Diffus.*, vol. 27, pp. 75–82, 2006.

[220] K. Haldar, B. Kiefer, and D. C. Lagoudas, "Finite element analysis of the demagnetization effect and stress inhomogeneities in magnetic shape memory alloy samples," *Phil. Mag.*, vol. 91, no. 32, pp. 4126–4157, 2011.

[221] A. K. Singh, S. Singh*, K. K. Dubey, P. Devi, P. Das, M. Etter, O. G. Grendal, C. Dejoie, A. Fitch, A. Senyshyn, S.-C. Lee, S. Bhattacharjee, and D. Pandey, "Evidence for Local Symmetry Breaking in the Skyrmion-Hosting Ni_2In-type Hexagonal Compounds." arXiv:2412.09158v1 [cond-mat.mtrl-sci].